Spring 5-1-2021

Spectroscopic Analysis of Potential Astromolecules Via Quantum Chemical Quartic Force Fields

Mason Gardner

SPECTROSCOPIC ANALYSIS OF POTENTIAL ASTROMOLECULES

VIA QUANTUM CHEMICAL QUARTIC FORCE FIELDS

By
Mason Bradford Gardner

A thesis submitted to the faculty of The University of Mississippi in partial fulfillment of the requirements of the Sally McDonnell Barksdale Honors College.

Oxford, MS
May 2021

Approved By

_____
Advisor: Professor Ryan Fortenberry

_____
Reader: Professor Nathan Hammer

_____
Reader: Professor Steven Davis

ABSTRACT

MASON BRADFORD GARDNER: Spectroscopic Analysis of Potential Astromolecules Via Quantum Chemical Quartic Force Fields

Astrochemistry has been substantially aided by computational techniques, particularly through the use of Quartic Force Field (QFF) analysis. Several methods have proven useful at correlating computed spectroscopic data with experimental observations. The F12-TZ QFF correlated well with experimental data for silicon oxide compounds, particularly those potentially involved in development from rocky bodies to planetary masses [27]. Compared to argon matrix experimental data, the vibrational frequencies for the molecules SiO_2, SiO_3, Si_2O_3, and Si_2O_4 become less accurate as the complexity of the molecules increases but should still be predictive of infrared characteristics of silicon oxides as they form clusters in space [27]. The CcCR QFF was found to be accurate for predicting B_0 and C_0 rotational constants within 35 MHz and vibrational frequencies within 5.7 cm^{-1} for many molecules, including those with heavy atoms [21]. When used in conjunction, the F12-TZ and CcCR QFFs produced parallel data for predicting the brightest vibrational frequencies in relatively complex molecules containing noble gases; rotational constants produced by the CcCR QFFs also present evidence for future identification of such molecules.

TABLE OF CONTENTS

LIST OF TABLES

LIST OF FIGURES AND EQUATIONS

FIGURES

EQUATIONS

LIST OF ABBREVIATIONS

SOFIA	Stratospheric Observatory for Infrared Astronomy
QFF	quartic force field
VPT2	second-order vibrational perturbation theory
CCSD(T)	coupled cluster theory at the singles, doubles, and perturbative triples level
F12-TZ	CCSD(T)-F12b/cc-pVTZ-F12
CcCR	CCSD(T)/CBS with core correlation and scalar relativity corrections
CBS	complete basis set extrapolation
MT	Martin-Taylor core correlating basis set
DK	Douglas-Kroll Hamiltonian
DFT	density functional theory analysis
JWST	James Webb Space Telescope
ZPVEs	zero-point vibrational energies
MAE	mean absolute error
MA%E	mean absolute percent errors

CHAPTER I: QUANTUM CHEMICAL ASTROCHEMISTRY

A. Introduction

Astrochemistry represents one of the widest fields of science encompassing a myriad of interrelated fields, including planetary geology, interstellar biology, and astronomy, not to mention the various subdisciplines of chemistry. Astrochemistry is directly concerned with the origin, abundance, and identity of molecules interacting in interstellar bodies, such as planets, stars, nebulae, etc. Originally, gas-phase experiments were conducted to compare observations between these "ground-based" experiments and spectroscopic data to determine the identity of astronomical molecules [1]; these determinations allow for conclusions and further research into chemical interactions in space and provide clues to astronomers as to the behavior of matter in these objects. Gas-phase experiments are a vital part of providing reliable and conclusive evidence about astrochemical data, but computational techniques offer solutions that expand the reach of astrochemistry [1].

Since the introduction of computational methods in chemistry, the abilities of astrochemists have grown substantially. By using quantum chemical theory to computationally design molecules and calculate their observables, a parallel option to gas-phase experiments is readily available and effective based on accuracy between theoretical calculations and physical experiment [1] with examples in Chapters II and III. As spectroscopy is the most dependable form of identifying molecules in space and the only available for remote sensing, the computational methods in this thesis are used to determine the spectroscopic data that would be observed under laboratory observations, specifically vibrational frequencies and rotational constants.

B. Spectroscopic Data

Vibrational spectroscopy measures the energy difference between quanta of molecular vibrational modes and are typically measured using infrared spectroscopy. Harmonic vibrational frequencies represent the energy differences that would be observed from molecules acting as perfect springs. However, molecules are anharmonic, and their energy levels vary significantly from harmonic modes. Specifically, anharmonic frequencies are usually lower than harmonic frequencies because the anharmonic, or Morse, behavior becomes asymptotic as bond length increases. Anharmonic vibrational frequencies are observed in spectroscopy, unlike harmonic vibrational frequencies. Hence, computational astrochemists must produce anharmonic vibrational frequencies for direct comparison to astronomical data [2].

Vibrational frequencies also have intensities, or brightness, if they have a change in dipole moment due to the vibration; these are infrared active frequencies. The intensity is also an observable characteristic of detectable astromolecules because it shows the activity levels of anharmonic vibrational modes, not harmonic modes [1] [3]. This is particularly noteworthy for the work reported in Chapter IV because of the high intensities exhibited by the noble gas structures.

Similarly, rotational constants affect the difference in energy between rotational states and are most often measured using microwave spectroscopy. These modes are just as unique as vibrational frequencies, and analyzing both of these observables makes astrochemical identification and analysis much more accurate than using either alone. Molecules have a rotational constant for each of the three principle axes—A, B, C. While linear molecules only have one rotational constant, noted as B, due to two degenerate and one infinite coordinate along the bonding plane. Rotational frequencies also follow a constant pattern based on the angular momentum while the step size between vibrational modes decreases with higher modes, an effect

of the anharmonic potential. In this way, rotational modes are easier to predict than vibrational modes [2].

Rotational and vibrational data can be used in conjunction as well. For example, vibrational frequencies are observed using infrared radiation, which is hindered by our planet's atmosphere; however, the microwave radiation used to observe rotational spectra are not hindered by the atmosphere. Therefore, rotational spectroscopy can be used first to determine where to direct the vibrational spectroscopes, improving the accuracy and decreasing the cost and errors occurring during vibrational studies. NASA uses this in its Stratospheric Observatory for Infrared Astronomy (SOFIA); SOFIA is an infrared spectroscope that is flown high into the sky in order to reduce the atmosphere's inhibition and to point the spectroscope in the direction previously determined by rotational spectroscopy [4].

C. Quartic Force Fields: F12-TZ and CcCR

Quartic force field (QFF) analysis involves a fourth-order Taylor series expansion of a molecule's equilibrium geometry to produce a potential energy surface, represented by the equation below. The "*F*" terms are force constants and "Δ" terms are displacements of the bond lengths by 0.005 Å and of the angles by 0.005 radians, respectively, within the molecule's optimized geometry:

$$V=\frac{1}{2}\left(\sum_{ij} F_{ij}\Delta_i\Delta_j\right)+\frac{1}{6}\left(\sum_{ijk} F_{ijk}\Delta_i\Delta_j\Delta_k\right)+\frac{1}{24}\left(\sum_{ijkl} F_{ijkl}\Delta_i\Delta_j\Delta_k\Delta_l\right). \quad (1)$$

This equation generates a potential energy surface of molecular displacements to find the minimum displaced geometry [5] [6]. Second-order vibrational perturbation theory (VPT2) uses the potential surface and force constants to calculate observable data about specific astromolecules, including the vibrational frequencies and rotational constants. QFFs have been

established as a reasonable method of determining these observables of molecules while maintaining a relatively low computational cost and high level of accuracy [7]. There are several available levels of theory to compute the desired spectroscopic data, and each has its own tradeoffs between cost and accuracy. The research in this thesis conducts QFFs based on coupled cluster theory at the singles, doubles, and perturbative triples (CCSD(T)) level [8] [9]. CCSD(T) QFFs follow a common procedure:

Step 1. Optimize molecular geometry
Step 2. Generate the displacements that define the QFF
Step 3. Calculate energies from displacements
Step 4. Fit potential energy surface
Step 5. Calculate anharmonic spectroscopic data
Step 6. Correct for resonances

Two kinds of QFFs are used in these projects: F12-TZ and CcCR, which are defined by their corresponding levels of theory discussed below. Chapter II discusses the use of F12-TZ QFFs in the study of silicon oxide compounds while Chapters III and IV discuss the use of CcCR QFFs in rotational constants and noble gas molecules, respectively.

Once a geometry for any designated molecule has been constructed and optimized, the computations can proceed. This is the same starting point for any QFF, and the level of theory is where the F12-TZ and CcCR QFFs begin diverging in technique [5].

Step 1. Optimize molecular geometry

The F12-TZ QFF relies on the "CCSD(T)-F12b/cc-pVTZ-F12" basis set, which is an F12 explicit electron correlation function with a triple zeta level basis set [10] [11]. Specifically, the geometry optimization uses the CCSD(T)-F12b/cc-pVTZ-F12 basis set [10] [11] in the quantum chemistry software package MOLPRO [12] [13], which is how this method gets its abbreviated name of "F12-TZ".

In contrast, CcCR QFFs optimize the geometry using canonical CCSD(T) with the aug-cc-pV5Z and Martin-Taylor (MT) basis sets in MOLPRO, whose complete descriptions are available in Table 1 below:

Table I.1: CcCR Geometry Optimization Basis Sets

Basis Set	**Abbreviation**
CCSD(T)/aug-cc-pV5Z	5Z
CCSD(T)/cc-pVTZ-MT with core electrons	MT_c
CCSD(T)/cc-pVTZ-MT without core electrons	MT

The Martin-Taylor basis sets are used to correct the impact that core electrons have on the geometry optimization [14]. The composite geometry is constructed by combing the 5Z geometry with the effect of the core electrons, found by the difference between MT_c and MT.

$$Composite = 5Z + MTc - MT. \quad (2)$$

Step 2. Generate the displacements that define the QFF

Once the bond angles and bond lengths of any designated molecule are optimized, every bond length and bond angle are subjected to individual displacements in every directional place, by 0.005 Å for the bond lengths and by 0.005 radians for the bond angles. Each molecular structure will have a different total number of displacements reflecting the number of atoms and bonds. These displacements are collected and converted into Cartesian coordinates for use in later programs.

Step 3. Calculate energies from displacements

Each displacement increases the molecule's potential energy, which can be calculated using various basis sets. The energy displacements in F12-TZ also use the "CCSD(T)-F12b/cc-pVTZ-F12" basis set [10] [11]. These energy displacements are calculated in MOLPRO [12] [13].

In the CcCR method, the composite geometry from above is used to generate seven sets of energy displacements, including a complete basis set extrapolation (CBS), Martin-Taylor basis set (MT) to correct for core electrons, and the Douglas-Kroll Hamiltonian (DK) to correct for scalar relativity [14] [15] [16]. The full basis sets are shown in Table 2 below. The CcCR name is representative of these energy displacements. The CBS energy is composed of 5Z, QZ, and TZ basis sets; the MT basis sets correct for core electrons; the DK basis sets correct for scalar relativity. This CCSD(T) computation can be summarized as CCSD(T)/CBS ("C") with core correlation corrections ("cC") and scalar relativity corrections ("R"), or "CcCR" when abbreviated all together [17].

Table I.2: CcCR Energy Displacements Basis Sets

Basis Set	**Abbreviation**
CCSD(T)/aug-cc-pV5Z	5Z
CCSD(T)/aug-cc-pVQZ	QZ
CCSD(T)/aug-cc-pVTZ	TZ
CCSD(T)/cc-pVTZ-MT with core electrons	MT_c
CCSD(T)/cc-pVTZ-MT without core electrons	MT
CCSD(T)/cc-pVTZ-DK with scalar relativity	DK_r
CCSD(T)/cc-pVTZ-DK without scalar relativity	DK

The energies from these calculations are recombined using Equation 3 below, where "E" represents the energy, "l" represents the angular momentum, and the exponential terms reflect the Taylor series expansion. This equation completes the CBS extrapolation, and is the best extrapolation scheme currently available [17].

$$E(l) = \left(5Z + QZ\left(l + \frac{1}{2}\right)^{-4} + TZ\left(l + \frac{1}{2}\right)^{-6}\right) + (MT_c - MT) + (DK_r - DK). \quad (3)$$

While these two methods follow a similar QFF methodology to determine spectroscopic data for these molecules, F12-TZ QFFs have a smaller computational cost based on the use of

explicit correlation and are quicker, while CcCR QFFs have a higher computational cost because they account for other molecular properties and include more levels of theory [18] [19] [20] [21].

Step 4. Fit potential energy surface

While the geometry optimization and energy displacements require different basis sets for F12-TZ and CcCR, the remaining steps are performed the same way. The single set of F12-TZ displacement energies are turned into relative energies based on the equilibrium energy, and these relative energies are then used to generate a potential energy surface in ANPASS using a least-squares procedure. The potential energy surface yields a new equilibrium geometry, and the force constants are found by refitting the potential to this geometry in ANPASS. Similarly, the components of the CcCR displacement energies are combined using Equation 3, made relative to the lowest combined energy, and fed into ANPASS in the same way described above [22].

Step 5. Calculate anharmonic spectroscopic data

The force constants and new equilibrium geometry are then collected for use by INTDER [23] and SPECTRO [24]. INTDER converts the internal coordinate force constants to Cartesian coordinates for use in SPECTRO [23]. SPECTRO completes the VPT2 and generates the observable harmonic and corrected anharmonic spectroscopic data [24] [25].

Step 6. Correct for resonances

This "raw" computed data is then used by SPECTRO again to correct for degenerative modes, Coriolis resonances, Fermi resonances, Darling-Dennison resonances, and potential Fermi-resonance polyads [26]. The results from this step produce the harmonic and corrected anharmonic spectroscopic data desired.

D. Applications

Both F12-TZ and CcCR QFFs can be applied to various astromolecules. As discussed in Chapter II, the F12-TZ QFF produces vibrational frequencies of silicon oxide compounds that were consistently within 7 cm^{-1} of argon-matrix experimentally observed frequencies [27]. Chapter III discusses the CcCR method, showing that this method accurately produced vibrational frequencies to within an average 5.8 cm^{-1} of experimental values for several small molecules known to be present in interstellar media [21]. In addition, CcCR rotational constants for the least anharmonic molecules are found to be accurate to within 34 MHz of experiment, and this accuracy is within the limit for directly observing these molecules in space [21]. Given the successful implementation of these QFFs in Chapters II and III, they are both utilized in Chapter IV. Molecules in Chapter IV are currently only theorized to exist as spectroscopic data has not yet been obtained for these molecules, but CcCR and F12-TZ produced similar data for these specific noble gas molecules, as discussed in Chapter IV.

Accuracies within 7 cm^{-1} of vibrational frequencies and 34 MHz of rotational constants support the idea that both the F12-TZ QFF and CcCR QFF blend speed and accuracy well for effectively predicting and comparing spectroscopic data to observations, while F12-TZ is slightly less accurate regarding rotational data [21] [27]. As interest in exotic and yet-to-be-observed interstellar molecules increases, many of these molecules will likely be difficult to synthesize for gas-phase experimental observation, making computational methods the best means to continue to generate highly accurate data for comparison to astronomical observation and exploration. By using computational methods in conjunction with physical experiments, the time and cost of arduous laboratory methods can be saved [1].

This research also has direct implications on knowledge of the universe. By comparing computational data to spectroscopic observations, astrochemists can make determinations about many interstellar bodies [1]. In Chapter II, silicon oxide molecules are the focal point because they are found in rocky bodies in space and form distinct clusters on the way to becoming larger bodies, such as comets and planets [27]. In Chapter III, the accuracy of rotational constants in CcCR QFFs for several small molecules are highlighted due to the inherent importance of and predictability of rotational constants in spectroscopy, showing that CcCR is effective and produces results similar to those of gas-phase experiments [21]. Chapter IV concerns the application of F12-TZ and CcCR QFFs to theoretical molecules with noble gas bonding, which could have implications on further research into noble gas bonding in new molecules. These methods can be used in many other studies, such as determining the age of stars, development of planets, and molecular composition of nebulae. Unifying computational astrochemistry with experimental spectroscopy can offer deeper insights in the chemistry of interstellar space and increase the imaginative potential of new molecules yet to be discovered [1].

CHAPTER II: SILICON OXIDES

Reprinted from [27]

Gardner, M. B.; Westbrook, B. R.; Fortenberry, R. C. Spectral Characterization for Small Clusters of Silicon and Oxygen: SiO2, SiO3, Si2O3, &; Si2O4. *Planetary and Space Science* 2020, *193*, 105076.

Spectral Characterization for Small Clusters of Silicon and Oxygen: SiO_2, SiO_3, Si_2O_3, & Si_2O_4

Mason B. Gardner

University of Mississippi, Department of Chemistry & Biochemistry, University, MS 38677, U.S.A.

Brent R. Westbrook

University of Mississippi, Department of Chemistry & Biochemistry, University, MS 38677, U.S.A.

Ryan C. Fortenberry*

University of Mississippi, Department of Chemistry & Biochemistry, University, MS 38677, U.S.A.

Abstract

Rocky bodies are made of minerals comprised largely of silicon and oxygen. How these minerals are formed from their constituent atoms is not fully known. The rovibrational IR spectral data produced in this work may help to observe small molecules containing silicon and oxygen so that these potential molecular intermediates can be observed. These molecules have strong absorption features between 7.0 μm and 8.0 μm, most notably, and are fully characterized in the IR from the present quantum chemical data. The antisymmetric Si−O stretches of small silicon oxide clusters also fall in this range and have large intensities. Hence, this quantum chemical analysis provides spectral data for such molecules that may be of significance for astrochemical classification and could play a role in the formation or degradation of mineral nanocrystals from or into their constituent atoms. Both explicitly computed anharmonic fundamental vibrational frequencies and those determined from scaled harmonic frequencies agree well with known experimental data, and spectroscopic constants are provided herein such that astronomical rotational spectral characterization may also be possible for the C_{2v} SiO_3 and Si_2O_3 molecules.

Keywords: Rovibrational spectroscopy; quantum chemistry; astrochemistry; planet formation

1. Introduction

Quartz, sand, and silica are all forms for the most abundant material in the Earth's crust and mantle. Crystalline SiO_2 gives way to the molten form deeper into the mantle, and it mixes with magnesium, iron, and aluminum to form most of the material present between the crust and core [1]. Similar processes likely played out all over the early Solar System and even beyond since both oxygen and silicon are two of the most abundant atoms in the Universe [2, 3, 4]. Consequently, there are few inorganic materials as common as silicon dioxide.

Silicon dioxide boils at nearly 3300 K and becomes isovalent with carbon dioxide in its triatomic molecular form. Such would likely be a necessary signature of silicon-based metabolism in exobiology. With regards to less exotic applications, silicates are known to condense under cold conditions creating rocky material in the first place [5], and these small molecules likely aggregate from silicon and oxygen atoms or the SiO monomer which has been observed in astrophysical environments since 1971 [6]. At the other end of the star's lifetime, the ablation of rocky materials as a star dies [7] or the stellar infall of most solid materials at any stage in a star's evolution will likely vaporize the crystalline or even molten silicates and quartzes creating small silicon oxide molecules for which little spectral data are well-known. A similar vaporization process would also take place terrestrially in foundries when high temperatures are utilized in large-scale industrial processes. Regardless of the circumstance, further spectral analysis of small silicon oxide clusters in the gas phase is necessary to produce data for the classification of silicon dioxide and its derivatives [8] such that the evolution of silicate materials from atoms to solids can be observed geophysically or industrially.

Argon matrix experiments have provided vibrational frequencies for the antisymmetric stretch and bending fundamentals of isolated SiO_2 at 1416 cm^{-1} and 273 cm^{-1}, respectively [9, 10, 11, 12]. Five of the six fundamental frequencies of SiO_3 have been ten-

*Corresponding author
Email address: r410@olemiss.edu (Ryan C. Fortenberry)

tatively assigned from similar experiments in conjunction with density functional theory analysis (DFT) [13], but follow-up work has not conclusively confirmed such attributions. Most notably, the a_1 O−O stretch could not be attributed experimentally from the DFT computations. The larger structures have been observed through photoelectron spectroscopy [14, 8], but the fundamental vibrational frequencies have not been conclusively determined in the laboratory. Three modes of Si_2O_4 have been reported in the literature again from argon matrix experiments [15], but there has been no experimental or high-level theoretical follow-up in the intervening 30 years. Granted, the gas phase data are likely similar to the argon matrix results in each of these studies since the argon should interact far less with the silicon and oxygen atoms than they would with hydrogens, for instance, but corroboration of some variety for these modes is still lacking. While some are better understood than others, the full vibrational spectra and especially gas-phase rotational constants for each these molecules are not fully classified.

Consequently, high-accuracy spectroscopic predictions for the vibrational frequencies of these molecules will enhance spectral models of environments where they may be found both in the laboratory and in nature. Quartic force fields (QFFs) are fourth-order Taylor series approximations to the potential portion of the internuclear Hamiltonian [16]. These have been shown to produce exceptional accuracy for determining anharmonic vibrational frequencies for relatively low computational cost, provided that a sufficient electronic structure method can be used to compute this specialized potential energy surface [16], most often coupled cluster theory at the singles, doubles, and perturbative triples [CCSD(T)][17, 18] level. The most accurate QFFs have produced vibrational frequencies to within 1 cm^{-1} on occasion and most often within 5-10 cm^{-1}. The accuracy of the rotational constants vary, but most are within 30 MHz of gas phase experiment [19, 20, 21, 22, 23, 24, 25, 26, 27, 28, 29, 30, 31].

However, the computational cost of this involved CCSD(T) approach including corrections for core electron correlation and complete basis set extrapolations is prohibitive for molecules containing more than five atoms. Recent work has shown that vibrational

frequencies of closed-shell molecules utilizing explicitly correlated CCSD(T)-F12b[32, 33] for the QFF energy points are within 7 cm^{-1} of the more expensive computations and cost orders of magnitude less time [34, 35, 36]. Some CCSD(T)-F12b anharmonic vibrational frequencies are actually closer to experiment than their more costly counterparts [35]. This approach has been utilized to predict anharmonic spectral data for $MgSiO_3$ and two isomers of Mg_2SiO_4 (enstatite and forsterite monomers, respectively) for which no previous vibrational or rotational spectroscopic data, theoretical or otherwise, exist [37]. Most notably these inorganic oxides produce very large infrared intensities implying that relatively small amounts of material could still be observed [38, 39, 37, 40]. Furthermore, other studies have produced scaling factors for harmonic frequencies of small, inorganic oxides that promise to reduce the computational time further for similar species in the production of accurate, anharmonic vibrational frequencies [40].

Regardless, the present work will extend the data for these geophysically- and astrochemically-relevant silicon oxides by computing the anharmonic vibrational frequencies and spectroscopic constants for four closed-shell singlet silicon oxide structures: SiO_2, SiO_3, Si_2O_3, and Si_2O_4. The D_{3h} structures of both CO_3 and SiO_3 have proven problematic in the past [41]. Here, only the C_{2v} SiO_3 structure, akin to its carbon analogue which performed well in recent QFF examination [42], is considered. While a four-membered ring isomer of Si_2O_3 is also known [43], we are leaving this structure for future study. The D_{2h} structure of Si_2O_4 has also been previously imposed to explain the results of photoelectron experiments [14] and the known vibrational frequencies thereof [15]. The rovibrational data provided herein will help to classify the building blocks or end products of silicates in regions where the solid form is known to exist [44, 7] especially with the growth in telescopic power most notably signified in the upcoming launch of the *James Webb Space Telescope (JWST).*

Figure 1: The optimized geometries and atom labels of A) SiO_2, B) SiO_3, C) Si_2O_3, and D) Si_2O_4.

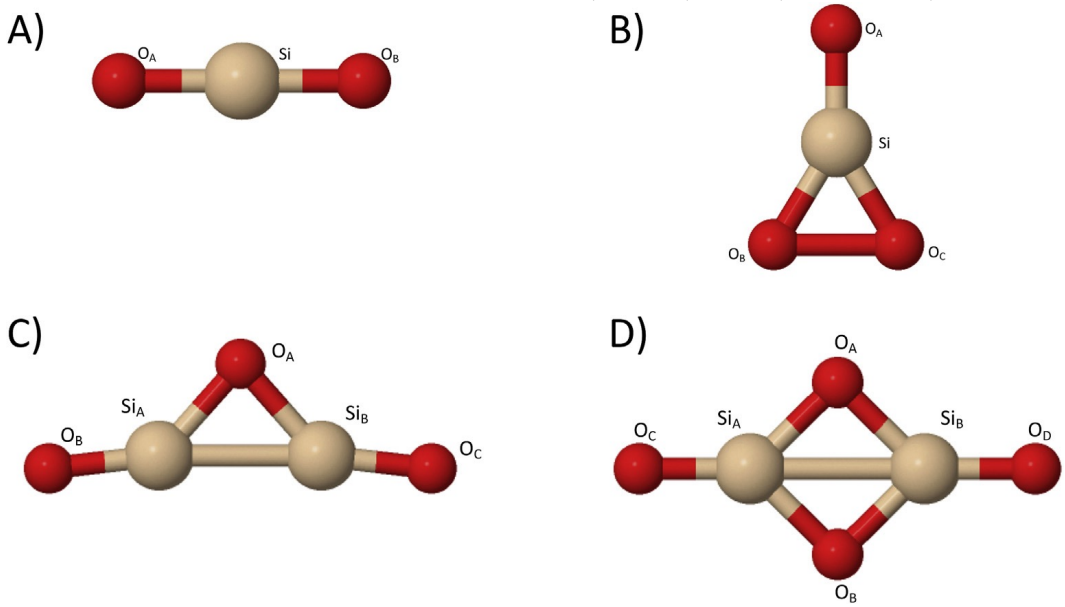

2. Computational Details

Precise optimization of the reference geometry is the first step to computing QFF-based anharmonic rovibrational data. The geometry optimization and all subsequent energy computations use CCSD(T)-F12b with the cc-pVTZ-F12 [45, 46] basis set (abbreviated as F12-TZ from here on) in MOLPRO2015.1 [47, 48]. The optimized geometry is then used to compute the harmonic vibrational frequencies within MOLPRO for comparison to those that result from the QFF. From the reference geometry of each silicon oxide molecule, coordinates are constructed to define the QFF with the bond lengths displaced by 0.005 Å and the bond angles and dihedrals displaced by 0.005 radians. Each of the four molecules has its own unique coordinate system since each has a different number of bond lengths, angles, and dihedrals giving different numbers of total points necessary for the QFF. SiO_2 has 57; SiO_3 has 413; Si_2O_3 has 1585; and Si_2O_4 has 1973 points. The coordinates for each system are defined below with atom labels in Figure 1.

The out-of-plane torsional modes are labeled as OPB. The coordinates for SiO_2:

$$S_1(\sigma_g) = \frac{1}{\sqrt{2}}[(Si - O_A) + (Si - O_B)] \tag{1}$$

$$S_2(\sigma_u) = \frac{1}{\sqrt{2}}[(Si - O_A) - (Si - O_B)] \tag{2}$$

$$S_3(\pi_u) = \angle(O_A - Si - O_B) \tag{3}$$

$$S_4(\pi_u) = \angle(O_A - Si - O_B); \tag{4}$$

SiO_3

$$S_1(a_1) = Si - O_A \tag{5}$$

$$S_2(a_1) = \frac{1}{\sqrt{2}}[(O_B - Si) + (O_C - Si)] \tag{6}$$

$$S_3(a_1) = \frac{1}{\sqrt{2}}[\angle(O_B - Si - O_A) + \angle(O_C - Si - O_A)] \tag{7}$$

$$S_4(b_2) = \frac{1}{\sqrt{2}}[(O_B - Si) - (O_C - Si)] \tag{8}$$

$$S_5(b_2) = \frac{1}{\sqrt{2}}[\angle(O_B - Si - O_A) - \angle(O_C - Si - O_A)] \tag{9}$$

$$S_6(b_1) = OPB(O_A - Si - O_B - O_C); \tag{10}$$

Si_2O_3

$$S_1(a_1) = Si_1 - Si_2 \tag{11}$$

$$S_2(a_1) = \frac{1}{\sqrt{2}}[(O_A - Si_A) + (O_A - Si_B)] \tag{12}$$

$$S_3(a_1) = \frac{1}{\sqrt{2}}[(Si_A - O_B) + (Si_B - O_C)] \tag{13}$$

$$S_4(a_1) = \frac{1}{\sqrt{2}}[\angle(O_B - Si_A - O_A) + \angle(O_C - Si_B - O_A)] \tag{14}$$

$$S_5(b_2) = \frac{1}{\sqrt{2}}[(O_A - Si_A) - (O_A - Si_B)] \tag{15}$$

$$S_6(b_2) = \frac{1}{\sqrt{2}}[(Si_A - O_B) - (Si_B - O_C)] \tag{16}$$

$$S_7(b_2) = \frac{1}{\sqrt{2}}[\angle(O_B - Si_A - O_A) - \angle(O_C - Si_B - O_A)] \tag{17}$$

$$S_8(b_1) = \frac{1}{\sqrt{2}}[\tau(O_B - Si_A - O_A - Si_B) - \tau(O_C - Si_B - O_A - Si_A)] \tag{18}$$

$$S_9(a_2) = \frac{1}{\sqrt{2}}[\tau(O_B - Si_A - O_A - Si_B) + \tau(O_C - Si_B - O_A - Si_A)]; \tag{19}$$

and Si_2O_4

$$S_1(a_g) = \frac{1}{\sqrt{2}}[(O_A - O_B) + (Si_A - Si_B)] \tag{20}$$

$$S_2(a_g) = \frac{1}{\sqrt{2}}[(O_A - O_B) - (Si_A - Si_B)] \tag{21}$$

$$S_3(a_g) = \frac{1}{\sqrt{2}}[(Si_A - O_C) + (Si_B - O_D)] \tag{22}$$

$$S_4(b_{1u}) = \frac{1}{2}[(O_A - Si_A) - (O_A - Si_B) - (O_B - Si_A) + (O_B - Si_B)] \tag{23}$$

$$S_5(b_{1u}) = \frac{1}{2}[\angle(O_C - Si_A - O_A) - \angle(O_C - Si_A - O_B) - \angle(O_D - Si_2 - O_A) + \angle(O_D - Si_B - O_B)] \tag{24}$$

$$S_6(b_{2u}) = \frac{1}{2}[(O_A - Si_A) + (O_A - Si_B) - (O_B - Si_A) - (O_B - Si_B)] \tag{25}$$

$$S_7(b_{2u}) = \frac{1}{2}[\angle(O_C - Si_A - O_A) + \angle(O_C - Si_A - O_B) - \angle(O_D - Si_2 - O_A) - \angle(O_D - Si_B - O_B)] \tag{26}$$

$$S_8(b_{3g}) = \frac{1}{\sqrt{2}}[(Si_A - O_C) - (Si_B - O_D)] \tag{27}$$

$$S_9(b_{3g}) = \frac{1}{2}[(O_A - Si_A) - (O_A - Si_B) + (O_B - Si_A) - (O_B - Si_B)] \tag{28}$$

$$S_{10}(b_{3u}) = \frac{1}{\sqrt{2}}[(O_C)_z + (O_D)_z] \tag{29}$$

$$S_{11}(b_{3u}) = \frac{1}{2}[(O_A)_z + (O_B)_z - (Si_A)_z - (Si_B)_z] \tag{30}$$

$$S_{12}(b_{2u}) = \frac{1}{\sqrt{2}}[(O_C)_z - (O_D)_z], \tag{31}$$

where the last of these three has exhibited some questionable results in the low-frequency range for the magnesium fluoride dimer [39]. The other coordinate systems have been utilized successfully in previous studies on the magnesium hydride monomer, $HeHHe^+$, carbon dioxide, CO_3, $NCNCN^-$, and C_2O_3 [39, 49, 42, 50].

The resulting energies are fit to a least-squares polynomial giving a sum of squared residuals on the order of 10^{-17} a.u.^{2} for all molecules but Si_2O_4 which is 10^{-13} a.u.^{2} This fit determines the actual minimum, or equilibrium, geometry. The final set of force constants are generated by refitting the points to this new minimum; these are given in the supplemental information (SI). The INTDER program [51] transforms these force constants into Cartesian coordinates for more general implementation. Then, the SPECTRO program [52] computes the harmonic and anharmonic frequencies including anharmonic zero-point vibrational energies (ZPVEs) using vibrational perturbation theory at second-order (VPT2) as well as spectroscopic constants making use of rotational

Table 1: The F12-TZ Vibrationally Averaged ($_0$) and Equilibrium ($_e$) Geometrical Parameters (in Å or Degrees) as Defined from Figure 1.

	SiO_2	SiO_3	Si_2O_3	Si_2O_4
r_0 (Si_A−O_A)	1.51249	1.50567	1.50675	1.50045
r_0 (Si_A−O_B)		1.62024	1.67351	1.66525[a]
$\angle_0$(O_A−Si_A−O_B)		148.675	137.445	90.544
r_0 (Si_A−Si_B)			2.21681	2.36644
$\angle_0$(O_A−Si_A−O_C)				135.326
r_e (Si_A−O_A)	1.51066	1.50395	1.50726	1.50337
r_e (Si_A−O_B)		1.61659	1.66903	1.66135[a]
$\angle_e$(O_A−Si_A−O_B)		148.814	137.313	90.673
r_e (Si_A−Si_B)			2.21069	2.36327
$\angle_e$(O_A−Si_A−O_C)				135.337

[a]This is actually $r_{e/0}$ (Si_A−O_C) because of the different atom labeling in Si_2O_4 but is placed here for consistency of bond type.

perturbation theory at second-order [53, 54, 55] and Fermi resonance polyads [56].

The B3LYP/aug-cc-pVDZ double-harmonic intensities and dipole moments are computed with Gaussian09 [57, 58, 59, 60, 61]. These have been shown to be in good agreement with higher-level computations previously [62, 63]. Additionally, the scaling factors for the Si-O stretching (0.98242) and bending (0.99261) frequencies determined previously [40] are applied to the harmonics computed directly in MOLPRO for comparison of their performance in these related but not identical systems.

3. Results & Discussion

The geometries for each of the four molecules examined here are given in Table 1 with labels from Figure 1. Most notably, the Si_A−O_A bond lengths, those that have the oxygen atom in a silaketone moiety (external Si=O group) are largely consistent with a bond length on the order of 1.5 Å. SiO_2 is the exception to this where the longer bond length likely arises from the weakening of the silicon atom's electron donation due to having two Si=O bonds instead of just one, and its magnitude here is in line with that computed previously [13]. The Si_A−$O_{B/C}$ bonds can be thought of as single bonds from a carbon analogue [42] and are notably and consistently longer. The Si−Si bonds are longer in Si_2O_4 than in Si_2O_3, but the additional oxygen atom in the former naturally increases the size of the ring thus making for a longer diagonal distance between silicon atoms.

Table 2: The F12-TZ Vibrational Frequencies (in cm^{-1}) and Intensities (in km/mol in parentheses) for SiO_2.

Mode	Description	Symm.	Harm. Freq.	Anharm. (QFF)	Scale Factor	Scaled	Exp.[a]	Δ(QFF-Scaled)
1	$1.00S_2$	σ_u	1439.7 (67)	1420.7	0.98242	1414.4	1416	6.3
2	$1.00S_1$	σ_g	992.4 (0)	984.2	0.98242	975.0		9.2
3	$1.00S_3$	π_u	290.6 (79)	289.0	0.99261	288.5	273	0.5
ZPVE			1361.4	1501.9				

[a]Argon matrix experimental data from [9, 10, 11, 12]

3.1. Anharmonic Frequencies

The F12-TZ vibrational frequencies for SiO_2 are given in Table 2. While the gas phase values for this molecule are not known, the argon matrix results correlate exceptionally well with the explicit QFF values for the 1420.7 cm^{-1} and 289.0 cm^{-1} fundamentals compared to the 1416 cm^{-1} and 273 cm^{-1} experimental frequencies [12]. Interestingly, the scaled 1414.4 cm^{-1} and 288.5 cm^{-1} frequencies for the same modes are in slightly closer agreement with experiment. Even so, the difference in the explicit QFF anharmonic frequencies and the scaled values are within the accuracy (7 cm^{-1}) of the F12-TZ approach implying that either is a valuable choice of method. The infrared inactive symmetric stretch has a larger difference between the two anharmonic frequencies, but no experimental data can verify which is more accurate. The F12-TZ QFF produces nearly identical values as gas-phase experimental CO_2 frequencies (differences of less than 2 cm^{-1} in every case) [42], and similar accuracies appear to be present in the silicon analogue, as well.

The strong correspondence between theory and argon matrix experiments continues with C_{2v} SiO_3. As shown in Table 3, the difference between the F12-TZ SiO_3 anharmonic frequencies and that for the argon matrix experiments[13] is never more than 8 cm^{-1}, and ν_3 at 857.1 cm^{-1} is within 2 cm^{-1} of experiment. Granted, the matrix will shift these values relative to the gas phase values that would be observed in astrophysical contexts, but, again, these shifts should be small. Furthermore, the B3LYP/aug-cc-pVTZ double-harmonic intensities are in at least semi-quantitative agreement with experiment

Table 3: The F12-TZ QFF Vibrational Frequencies (in cm^{-1}) and Intensities (in km/mol in parentheses) for C_{2v} SiO_3.

Mode	Description	Symm.	Harm. Freq.	Anharm. (QFF)	Scale Factor	Scaled	Exp.[a]	Δ(QFF-Scaled)
1	$0.71S_1 + 0.29S_2$	a_1	1391.4 (114)	1371.0	0.98242	1366.9	1363.5 (100)	4.1
2	$0.72S_2 + 0.27S_1$	a_1	894.2 (5)	885.3	0.98242	878.5	877.1 (12)	6.8
3	$1.00S_4$	b_2	868.5 (90)	857.1	0.98242	853.2	855.3 (53)	3.9
4	$1.00S_3$	a_1	515.0 (25)	497.0	0.99261	511.2	–	-14.2
5	$1.00S_6$	b_1	309.7 (82)	305.3	0.99261	307.4	287.8 (96)	-2.1
6	$1.00S_5$	b_2	299.3 (60)	298.0	0.99261	297.1	292.0 (62)	0.9
ZPVE			2139.1	2129.5				

[a] Argon matrix data from [13].

showing which bands could be considered strong and which could be considered weak. Unsurprisingly, the ν_1 terminal Si=O_A stretch at 1371.0 cm^{-1} is the brightest vibrational mode, and the OPB bend for O_A is also bright lining up with experiment.

The previous SiO_3 experiment could not identify the a_1 ν_4 symmetric bend (equivalently described as the O−O stretch). This fundamental has an intensity greater than the ν_2 Si−O symmetric stretch previously characterized in the argon matrix experiments [13]. The reason is likely that the previous DFT computations suggested that the fundamental should lie higher in frequency close to 582 cm^{-1}. However, the present work strongly suggests that this fundamental is much lower in frequency at 497.0 cm^{-1}. Unfortunately, this region of the IR spectrum is not reported in this previous work negating any *ex post facto* analysis. Regardless, the F12-TZ QFF values confirm the other argon matrix fundamental vibrational frequency assignments for C_{2v} SiO_3[13] and show that the last remaining band is most likely lower in frequency than previously believed.

Table 4: Si_2O_3 F12-TZ Harmonic and Fundamental Vibrational Frequencies (in cm^{-1}) and Intensities (in km/mol in parentheses).

Mode	Description	Symm.	Harm. Freq.	Anharm. (QFF)	Scale Factor	Scaled	Δ(QFF-Scaled)
1	$0.86S_3+0.08S_2+0.07S_1$	a_1	1331.0 (17)	1303.3	0.98242	1307.6	-4.3
2	$0.96S_6+0.04S_5$	b_2	1274.0(152)	1245.6	0.98242	1251.6	-6.0
3	$0.85S_2+0.08S_4+0.07S_3$	a_1	859.1(122)	836.2	0.98242	844.0	-7.8
4	$0.88S_5+0.07S_7+0.05S_6$	b_2	663.2(52)	637.6	0.98242	651.6	14.0
5	$0.74S_1+0.18S_4+0.07S_3$	a_1	440.7(21)	432.5	0.99261	437.5	-5.0
6	$0.93S_7+0.08S_5$	b_2	248.7(16)	245.0	0.99261	246.9	-1.9
7	$1.00S_9$	b_1	245.7(62)	244.6	0.99261	243.9	0.7
8	$0.74S_4+0.19S_1+0.07S_2$	a_1	189.8(30)	188.2	0.99261	188.4	-0.2
9	$1.00S_8$	a_2	153.4(0)	153.7	0.99261	152.3	1.4
ZPVE			2643.3	2679.5			

The F12-TZ QFF fundamental vibrational frequencies for Si_2O_3 have not been previously explored experimentally or theoretically and are given here in Table 4. The silaketone stretches (ν_1 and ν_2) are in the same frequency range as that for SiO_3, and the antisymmetric ν_2 stretch at 1245.6 cm^{-1} has the greatest intensity of all the fundamentals. This is also true for the related C_2O_3 and $C_2N_3^-$ molecules [42, 50]. The a_1 ν_3 stretching of the central O_A atom produces the next-brightest fundamental at 836.2 cm^{-1}. The permanent dipole moment is being extended in this case, giving a larger charge separation upon vibration. The remaining frequencies are dimmer but still non-negligible, and the five lowest frequency fundamentals are all below 500 cm^{-1}, as is common for such heavy atoms like silicon [38, 39, 37].

Table 5: Si_2O_4 F12-TZ Harmonic and Fundamental Vibrational Frequencies (in cm^{-1}) and Intensities (in km/mol in parentheses).

Mode	Description	Symm.	Harm. Freq.	Anharm. (QFF)	Scale Factor	Scaled	Exp.[a]	Δ(QFF-Scaled)
1	$0.84S_3$+$0.13S_1$	a_g	1354.4 (0)	1338.2	0.98242	1330.6		7.6
2	$0.86S_8$+$0.14S_9$	b_{3g}	1316.9 (382)	1303.6	0.98242	1293.7	1293.3	9.9
3	$0.89S_6$+$0.11S_7$	b_{2u}	904.8 (259)	911.7	0.98242	888.9	889.2	22.8
4	$0.70S_1$+$0.24S_2$+$0.06S_3$	a_g	871.6 (0)	861.3	0.98242	856.3		5.0
5	$0.86S_9$+$0.14S_8$	b_{3g}	804.0 (252)	856.8	0.98242	789.9	786.4	66.9
6	$1.00S_4$	b_{1u}	718.7 (0)	658.1	0.98242	706.1		-48.0
7	$0.73S_2$+$017S_1$+$0.10S_3$	a_g	488.0 (0)	485.9	0.98242	479.4		6.5
8	$0.94S_11$+$0.06S_10$	b_{3u}	465.4 (99)	456.1	0.99261	462.0		-5.9
9	$1.00S_5$	b_{1u}	313.3 (0)	281.7	0.99261	311.0		-29.3
10	$0.89S_7$+$0.11S_6$	b_{2u}	295.5† (43)		0.99261	293.3		
11	$1.00S_12$	b_{2u}	236.6 (0)	230.5	0.99261	234.9		-4.4
12	$0.94S_10$+$0.06S_11$	b_{3u}	121.5† (26)		0.99261	120.6		
ZPVE			3945.4	3796.3				

[a] Argon matrix experimental results from [15].
† Denotes a MOLPRO harmonic frequency

The 12 fundamental vibrational frequencies for D_{2h} Si_2O_4 are given in Table 5. The silaketone stretches are blue-shifted in this molecule compared to Si_2O_3 and are present above 1300 cm^{-1}. The b_{3g} ν_2 antisymmetric stretch, again, has the largest intensity of all the fundamental frequencies for this molecule. Stretches within the ring (ν_3 and ν_5) are the next-brightest with intensities above 250 km/mol, more than 3.5 times that of the antisymmetric stretch in water. Comparison to argon matrix data from [15] gives good agreement between the 1293.3 cm^{-1} value and the F12-TZ QFF ν_2 frequency at

1303.6 cm^{-1}. This deteriorates slightly for ν_3 where experiment places this at 889.2 cm^{-1} and the QFF is 911.7 cm^{-1}. The correlation is completely off for ν_5 with experiment attributing this ring deformation to a band at 786.4 cm^{-1} and the QFF at 856.8 cm^{-1}. Either the band has been misassigned in the experiment, or the computations are off.

In this case, the latter is most likely correct. The fitting of the points was the worst for Si_2O_4 of the silicon oxides studied. Furthermore, two harmonic vibrational frequencies computed via the QFF do not align with those computed from within MOLPRO's standard harmonic frequency computation, ω_{10} and ω_{12}. The OPB coordinate struggles to define the proper motion within the constraints of the QFF and VPT2, and this subsequently affects the fitting of the force constants for the other coordinates. The potential for the OPB is likely flat reducing the capabilities of VPT2 as defined by the QFF. The ν_{10} and ν_{12} fundamentals could not even be computed from the QFF data. Hence, the F12-TZ QFF VPT2 anharmonic vibrational frequencies for Si_2O_4 below the silaketone stretches should be treated as suggestions.

However, all is not lost in the prediction of these anharmonic frequencies. The recent determination of scaling factors for M−O stretches and bends (where M is a second-row atom) can be applied to Si_2O_4. Doing so actually produces a fundamental frequency for ν_3 at 888.9 $cm^{-1}$and ν_5 at 789.9 cm^{-1}. Both are within 3.5 cm^{-1} of the argon matrix experiment. Furthermore, the ν_2 antisymmetric stretch is 1293.7 cm^{-1} from the scaled values, 9.9 cm^{-1} below the explicit QFF, and only 0.4 cm^{-1} below the experimental value. Consequently, the scaled harmonics are likely producing more meaningful fundamental vibrational frequencies for this molecule than the QFF. The harmonic force field is much better behaved and less likely to suffer from noise contamination in these numerical derivatives [19, 20], and the amount of absolute anharmonicity is relatively small in the first place.

The scaled harmonic frequencies are also listed for the other three molecules giving slightly better correlation with experiment for SiO_2 (Table 2) as discussed previously. Agreement between experiment and scaled harmonics of SiO_3 (Table 3) is comparable

with the F12-TZ QFF VPT2 results. Some modes are better with the scaled values (ν_1) and some with the explicit anharmonicity computed (ν_3) implying that either is appropriate. Both also demonstrate that ν_4 is still lower in frequency than previous experiments explored. Since there are no experimental data for Si_2O_3, comparison between the QFF VPT2 results and the scaled harmonics both with F12-TZ is necessary, but both are quite comparable with one another (Table 4). All modes agree to within 8 cm^{-1} save for the b_2 ν_4 antisymmetric stretch. The mean absolute error (MAE) between the QFF and scaled harmonics for the stretching frequencies is 5.8 cm^{-1} when removing ν_4 and 8.0 cm^{-1} when including it. The bends and torsions are much closer with the MAE at 1.8 cm^{-1}, but, again, the magnitudes of the frequencies are smaller in the first place. Hence, these scaling factors are comparable to the QFF VPT2 fundamental vibrational frequencies implying that these heuristics could be used as a first-order guess to the fundamental vibrational frequencies of Si_2O_4 and potentially even for larger silicon oxide clusters where QFFs or any anharmonic vibrational frequency computations are prohibitively large.

3.2. Rotational and Spectroscopic Constants

The spectroscopic constants for each of the molecules examined are given in Table 6. These include the pure rotational constants, the vibrationally-averaged rotational constants, the quartic and sextic (Watson S Hamiltonian) distortion constants, and even the dipole moments of the two C_{2v} molecules. While these may not be as accurate as methods including core electron correlation or other additive factors [35, 36], these rotational constants should serve as a good starting point for assessing the rotational spectra of these molecules. Strangely, a search of the literature did not yield any experimental rotational constants for SiO_2 which are provided here for this nonpolar molecule. The other three molecules are all clearly near-prolate rotors especially for Si_2O_3.

The vibrationally-excited rotational constants (numbered in the same order as the fundamental vibrational frequencies) for Si_2O_4 are given for the modes with the least questionable vibrational frequencies. While the pure rotational transitions of this molecule

Table 6: The F12-TZ QFF Spectroscopic Data for the Four Silicon Oxides.

	SiO_2	SiO_3	Si_2O_3	Si_2O_4
A_0 (MHz)		22360.3	21364.6	11474.0
B_0 (MHz)	6907.7	5489.9	1766.6	1636.1
C_0 (MHz)		4400.5	1630.8	1433.1
A_1 (MHz)		22333.1	21390.3	11469.1
B_1 (MHz)	6872.3	5466.1	1761.6	1632.6
C_1 (MHz)		4384.4	1626.6	1430.4
A_2 (MHz)		22292.4	21361.1	11465.8
B_2 (MHz)	6888.1	5480.1	1762.9	1633.0
C_2 (MHz)		4392.0	1627.6	1430.8
A_3 (MHz)		22446.5	21282.1	11497.3
B_3 (MHz)	6920.3	5469.6	1764.8	1633.3
C_3 (MHz)		4391.4	1628.1	1430.4
A_4 (MHz)		22001.5	20997.0	11458.5
B_4 (MHz)		5518.5	1768.1	1635.0
C_4 (MHz)		4392.3	1629.6	1431.8
A_5 (MHz)		22310.3	21576.9	11442.8
B_5 (MHz)		5493.9	1761.6	1635.2
C_5 (MHz)		4409.0	1627.2	1431.5
A_6 (MHz)		22408.0	21370.4	11446.5
B_6 (MHz)		5504.1	1768.2	1633.6
C_6 (MHz)		4400.9	1631.2	1430.7
A_7 (MHz)			21368.9	
B_7 (MHz)			1767.8	
C_7 (MHz)			1632.6	
A_8 (MHz)			21507.1	
B_8 (MHz)			1767.9	
C_8 (MHz)			1630.7	
A_9 (MHz)			21279.8	
B_9 (MHz)			1768.2	
C_9 (MHz)			1633.4	
Δ_J (Hz)	1.500	941.78	120.62	56.658
Δ_K (kHz)		133.62	363.47	9.985
Δ_{JK} (kHz)		15.616	-4.444	0.389
δ_J (Hz)		227.57	18.119	8.426
δ_K (kHz)		11.708	1.065	0.484
Φ_J (μHz)	-8.885	518.99	2.540	2.770
Φ_K (Hz)		-0.240	9.387	0.022
Φ_{JK} (mHz)		80.382	0.920	0.242
Φ_{KJ} (mHz)		-233.60	-127.77	-4.098
ϕ_j (μHz)		261.21	4.481	1.058
ϕ_{jk} (mHz)		45.749	0.152	0.152
ϕ_k (Hz)		1.292	0.502	0.009
μ (D)	–	0.87	0.66	–

will not be observed since it has no dipole moment, the A_2, B_2, and C_2 values, however, will likely be important for rovibrational modeling since ν_2 of this molecule has the largest infrared intensity computed of the set. Finally, the dipole moments are reported at the bottom of Table 6. SiO_3 is the most polar, but Si_2O_3 has a smaller but similar magnitude dipole moment. This differs from the carbon analogues where C_2O_3 is almost apolar [42] likely due to the larger electronegativity difference between oxygen and silicon as well as the longer Si−O bonds.

4. Conclusions

The small silicon oxide clusters SiO_2, SiO_3, Si_2O_3, and Si_2O_4 are shown here to be stable species with notably bright mid- to far-IR active fundamental vibrational frequencies. The antisymmetric silaketone stretch in the silicon dioxide dimer has the largest intensity of the set. The range between 1420 cm^{-1} and 1250 cm^{-1} (7.0 μm and 8.0 μm) contains this most intense band and its counterparts from the other three oxides. The other infrared bands typically fall below 700 cm^{-1} (>14.3 μm) with many of the silicon oxides analyzed here having one or two bands around 850 cm^{-1} ($\sim$11.8 μm). Each of these regions have notable bumps from astronomical spectra [64], implying that small, geochemically-relevant silicon oxides may be present in circumstellar media and protoplanetary disks. Upcoming *JWST* spectra could potentially resolve such peaks. Furthermore, the larger molecules have infrared features approaching that of known silicate dusts. The polar SiO_3 and Si_2O_3 clusters could be observed from the ground with radiotelescopes, and the present data will aid in the experimental characterization necessary to provide reference data for such observations.

Additionally, the previously derived scaling factors [40] show promise in treating similar inorganic oxides that are intractable for QFF computations. Comparison to experimental spectra for SiO_2 and SiO_3 shows that both the explicit anharmonic computations and the scaled harmonics are similarly accurate partly due to the small magnitudes of the anharmonicities of the molecules examined. However, these scaled harmonics also do

not suffer from coordinate issues observed in Si_2O_4 making them also potentially useful for future exploration of larger mineralogically-relevant inorganic oxides.

Acknowledgements

The authors acknowledge funding from the NSF (OIA-1757220), NASA (NNX17AH15G), and the University of Mississippi start-up funds.

References

[1] White, W. M. *Geochemistry*, 1st ed.; Wiley: Hoboken, NJ, 2013; Chapter 10: The Big Picture: Cosmochemistry.

[2] Savage, B. D.; Sembach, K. R. Interstellar Abundances from Absorption-Line Observations with the *Hubble Space Telescope*. *Annu. Rev. Astron. Astrophys.* **1996**, *34*, 279–329.

[3] McCall, B. J. Dissociative Recombination of Cold H_3^+ and Its Interstellar Implications. *Phil. Trans. Royal Soc. A* **2006**, *364*, 2953–2963.

[4] Fortenberry, R. C. The Case for Gas-Phase Astrochemistry without Carbon. *Mol. Astrophys.* **2020**, *18*, 100062.

[5] Rouillé, G.; Jäger, C.; Krasnokutski, S. A.; Krebszb, M.; Henning, T. Cold Condensation of Dust in the ISM. *Farad. Discuss.* **2014**, *168*, 449–460.

[6] Wilson, R. W.; Penzias, A. A.; Jefferts, K. B.; Kutner, M.; Thaddeus, P. Discovery of Interstellar Silicon Monoxide. *Astrophys. J.* **1971**, *167*, L97–L100.

[7] McCarthy, M. C.; Gottlieb, C. A.; Cernicharo, J. Building Blocks of Dust: A Coordinated Laboratory and Astronomical Study of the Archtype AGB Carbon Star IRC+10216. *J. Molec. Spectrosc.* **2019**, *356*, 7–20.

[8] Wang, L.-S.; Desai, S. R.; Wu, H.; Nicholas, J. B. Small Silicon Oxide Clusters: Chains and Rings. *Z. Phys. D* **1997**, *40*, 36–39.

[9] Schnöckel, H. IR Spectroscopic Detection of Molecular SiO_2. *Angew. Chem. Int. Ed. Engl.* **1978**, *17*, 616–617.

[10] Schnöckel, V. H. Matrixreaktionen von SiO. IR-spektroskopischer Nachweis der Molekeln SiO_2 und $OSiCl_2$. *Z. Anorg. Allg. Chem.* **1980**, *460*, 37–50.

[11] Andrews, L.; McCluskey, M. Bending Modes of SiO_2 and GeO_2 in Solid Argon. *J. Mol. Spectrosc.* **1992**, *154*, 223–225.

[12] Jacox, M. E. Vibrational and Electronic Energy Levels of Polyatomic Transient Molecules. *J. Phys. Chem. Ref. Data* **1994**, *23*, 1–461.

[13] Tremblay, B.; Roy, P.; Manceron, L.; Alikhani, M. E.; Roy, D. Vibrational Spectrum and Structure of Silicon Trioxide SiO_3: A Matrix Isolation Infrared and Density Functional Theory Study. *J. Chem. Phys.* **1996**, *104*, 2773–2781.

[14] Wang, L.-S.; Wu, H.; Desai, S. R.; Fan, J.; Colson, S. D. A Photoelectron Spectroscopic Study of Small Silicon Oxide Clusters: SiO_2, Si_2O_3, and Si_2O_4. *J. Phys. Chem.* **1996**, *100*, 8697–8700.

[15] Mehner, T.; Göckes, H. J.; Schunck, S.; Schnöckel, H. Dimeres SiO_2 Matrix-IR-Untersuchungen und ab Initio SCF-Rechnungen. *Z. Anorg. Allg. Chem.* **1980**, *580*, 121–130.

[16] Fortenberry, R. C.; Lee, T. J. Computational Vibrational Spectroscopy for the Detection of Molecules in Space. *Ann. Rep. Comput. Chem.* **2019**, *15*, 173–202.

[17] Raghavachari, K.; Trucks, G. W.; Pople, J. A.; Head-Gordon, M. A Fifth-Order Perturbation Comparison of Electron Correlation Theories. *Chem. Phys. Lett.* **1989**, *157*, 479–483.

[18] Shavitt, I.; Bartlett, R. J. *Many-Body Methods in Chemistry and Physics: MBPT and Coupled-Cluster Theory*; Cambridge University Press: Cambridge, 2009.

[19] Huang, X.; Lee, T. J. A Procedure for Computing Accurate *Ab Initio* Quartic Force Fields: Application to HO_2^+ and H_2O. *J. Chem. Phys.* **2008**, *129*, 044312.

[20] Huang, X.; Lee, T. J. Accurate *Ab Initio* Quartic Force Fields for NH_2^- and CCH^- and Rovibrational Spectroscopic Constants for Their Isotopologs. *J. Chem. Phys.* **2009**, *131*, 104301.

[21] Huang, X.; Taylor, P. R.; Lee, T. J. Highly Accurate Quartic Force Field, Vibrational Frequencies, and Spectroscopic Constants for Cyclic and Linear $C_3H_3{}^+$. *J. Phys. Chem. A* **2011**, *115*, 5005–5016.

[22] Fortenberry, R. C.; Huang, X.; Francisco, J. S.; Crawford, T. D.; Lee, T. J. The *trans*-HOCO Radical: Fundamental Vibrational Frequencies, Quartic Force Fields, and Spectroscopic constants. *J. Chem. Phys.* **2011**, *135*, 134301.

[23] Fortenberry, R. C.; Huang, X.; Francisco, J. S.; Crawford, T. D.; Lee, T. J. Vibrational Frequencies and Spectroscopic Constants from Quartic Force Fields for *cis*-HOCO: The Radical and the Anion. *J. Chem. Phys.* **2011**, *135*, 214303.

[24] Fortenberry, R. C.; Huang, X.; Francisco, J. S.; Crawford, T. D.; Lee, T. J. Fundamental Vibrational Frequencies and Spectroscopic Constants of $HOCS^+$, $HSCO^+$, and Isotopologues via Quartic Force Fields. *J. Phys. Chem. A.* **2012**, *116*, 9582–9590.

[25] Huang, X.; Fortenberry, R. C.; Lee, T. J. Protonated Nitrous Oxide, $NNOH^+$: Fundamental Vibrational Frequencies and Spectroscopic Constants from Quartic Force Fields. *J. Chem. Phys.* **2013**, *139*, 084313.

[26] Fortenberry, R. C.; Huang, X.; Crawford, T. D.; Lee, T. J. Quartic Force Field Rovibrational Analysis of Protonated Acetylene, $C_2H_3{}^+$, and Its Isotopologues. *J. Phys. Chem. A* **2014**, *118*, 7034–7043.

[27] Zhao, D.; Doney, K. D.; Linnartz, H. Laboratory Gas-Phase Detection of the Cyclopropenyl Cation (c-$C_3H_3{}^+$). *Astrophys. J. Lett.* **2014**, *791*, L28.

[28] Fortenberry, R. C.; Lee, T. J.; Müller, H. S. P. Excited Vibrational Level Rotational Constants for SiC_2: A Sensitive Molecular Diagnostic for Astrophysical Conditions. *Molec. Astrophys.* **2015**, *1*, 13–19.

[29] Kitchens, M. J. R.; Fortenberry, R. C. The Rovibrational Nature of Closed-Shell Third-Row Triatomics: HOX and HXO, X = Si^+, P, S^+, and Cl. *Chem. Phys.* **2016**, *472*, 119–127.

[30] Fortenberry, R. C. Quantum Astrochemical Spectroscopy. *Int. J. Quant. Chem.* **2017**, *117*, 81–91.

[31] Bizzocchi, L.; Lattanzi, V.; Laas, J.; Spezzano, S.; Giuliano, B. M.; Prudenzano, D.; Endres, C.; Sipilä, O.; Caselli, P. Accurate Sub-millimetre Rest Frequencies for $HOCO^+$ and $DOCO^+$ Ions. *Astron. Astrophys.* **2017**, *602*, A34.

[32] Adler, T. B.; Knizia, G.; Werner, H.-J. A Simple and Efficient CCSD(T)-F12 Approximation. *J. Chem. Phys.* **2007**, *127*, 221106.

[33] Knizia, G.; Adler, T. B.; Werner, H.-J. Simplified CCSD(T)-F12 Methods: Theory and Benchmarks. *J. Chem. Phys.* **2009**, *130*, 054104.

[34] Agbaglo, D.; Lee, T. J.; Thackston, R.; Fortenberry, R. C. A Small Molecule with PAH Vibrational Properties and a Detectable Rotational Spectrum: c-(C)C_3H_2, Cyclopropenylidenyl Carbene. *Astrophys. J.* **2019**, *871*, 236.

[35] Agbaglo, D.; Fortenberry, R. C. The Performance of CCSD(T)-F12/aug-cc-pVTZ for the Computation of Anharmonic Fundamental Vibrational Frequencies. *Int. J. Quantum Chem.* **2019**, *119*, e25899.

[36] Agbaglo, D.; Fortenberry, R. C. The Performance of Explicitly Correlated Wavefunctions [CCSD(T)-F12b] in the Computation of Anharmonic Vibrational Frequencies. *Chem. Phys. Lett.* **2019**, *734*, 136720.

[37] Valencia, E. M.; Worth, C. J.; Fortenberry, R. C. Enstatite ($MgSiO_3$) and Forsterite (Mg_2SiO_4) Monomers and Dimers: Highly-Detectable Infrared and Radioastronomical Molecular Building Blocks. *Mon. Not. Royal Astron. Soc.* **2020**, *492*, 276–282.

[38] Kloska, K. A.; Fortenberry, R. C. Gas-Phase Spectra of MgO Molecules: A Possible Connection from Gas-Phase Molecules to Planet Formation. *Mon. Not. Royal Astron. Soc.* **2018**, *474*, 2055–2063.

[39] Palmer, C. Z.; Fortenberry, R. C. Rovibrational Considerations for the Monomers and Dimers of Magnesium Hydride (MgH_2) and Magnesium Fluoride (MgF_2). *J. Phys. Chem. A* **2018**, *122*, 7079–7088.

[40] Westbrook, B. R.; Fortenberry, R. C. Anharmonic Frequencies of $(MO)_2$ & Related Hydrides for M = Mg, Al, Si, P, S, Ca, & Ti and Heuristics for Predicting Anharmonic Corrections of Inorganic Oxides. *J. Phys. Chem. A* **2020**, *124*, 3191–3204.

[41] Beste, A.; Bartlett, R. J. The Electronic Structure of SiO_3: A Problematic Example for Coupled Cluster Methods. *Chem. Phys. Lett.* **2002**, *366*, 100–108.

[42] Fortenberry, R. C.; Peters, D.; Ferari, B. C.; Bennett, C. J. Rovibrational Spectral Analysis of CO_3 and C_2O_3: Potential Sources for O_2 Observed in Comet 67P/Churyumov-Gerasimenko. *Astrophys. J. Lett.* **2019**, *886*, L10.

[43] Wang, Y.; Chen, M.; Xie, Y.; Wei, P.; Schaefer, III, H. F.; von R. Schleyer, P.; Robinson, G. H.

Stabilization of Elusive Silicon Oxides. *Nature Chem.* **2015**, *7*, 509–513.
[44] Rho, J.; Gomez, H. L.; Boogert, A.; Smith, M. W. L.; Lagage, P.-O.; Dowell, D.; Clark, C. J. R.; Peeters, E.; Cami, J. A Dust Twin of Cas A: Cool Dust and 21 μm Silicate Dust Feature in the Supernova Remnant G54.1+0.3. *Mon. Not. Royal Astron. Soc.* **2018**, *479*, 5101–5123.
[45] Hill, J. G.; Peterson, K. A. Correlation Consistent Basis Sets for Explicitly Correlated Wavefunctions: Valence and Core-Valence Basis Sets for Li, Be, Na, and Mg. *Phys. Chem. Chem. Phys.* **2010**, *12*, 10460–10468.
[46] Prascher, B. P.; Woon, D. E.; Peterson, K. A.; Dunning, T. H.; Wilson, A. K. Gaussian Basis Sets for Use in Correlated Molecular Calculations. VII. Valence, Core-Valence, and Scalar Relativistic Basis Sets for Li, Be, Na, and Mg. *Theor. Chem. Acc.* **2011**, *128*, 69–82.
[47] Werner, H.-J. et al. MOLPRO, Version 2015.1, a Package of *ab Initio* Programs. 2015; see http://www.molpro.net.
[48] Werner, H.-J.; Knowles, P. J.; Knizia, G.; Manby, F. R.; Schütz, M. Molpro: A General-Purpose Quantum Chemistry Program Package. *WIREs Comput. Mol. Sci.* **2012**, *2*, 242–253.
[49] Stephan, C. J.; Fortenberry, R. C. The Interstellar Formation and Spectra of the Noble Gas, Proton-Bound $HeHHe^+$, $HeHNe^+$ and $HeHAr^+$ Complexes. *Mon. Not. Royal Astron. Soc.* **2017**, *469*, 339–346.
[50] Dubois, D.; Sciamma-O'Brien, E.; Fortenberry, R. C. The Fundamental Vibrational Frequencies and Spectroscopic Constants of the Dicyanoamine Anion, $NCNCN^-$ ($C_2N_3{}^-$): Quantum Chemical Analysis for Astrophysical and Planetary Environments. *Astrophys. J.* **2019**, *883*, 109.
[51] Allen, W. D.; coworkers, 2005; *INTDER* 2005 is a General Program Written by W. D. Allen and Coworkers, which Performs Vibrational Analysis and Higher-Order Non-Linear Transformations.
[52] Gaw, J. F.; Willets, A.; Green, W. H.; Handy, N. C. In *Advances in Molecular Vibrations and Collision Dynamics*; Bowman, J. M., Ratner, M. A., Eds.; JAI Press, Inc.: Greenwich, Connecticut, 1991; pp 170–185.
[53] Mills, I. M. In *Molecular Spectroscopy - Modern Research*; Rao, K. N., Mathews, C. W., Eds.; Academic Press: New York, 1972; pp 115–140.
[54] Watson, J. K. G. In *Vibrational Spectra and Structure*; During, J. R., Ed.; Elsevier: Amsterdam, 1977; pp 1–89.
[55] Papousek, D.; Aliev, M. R. *Molecular Vibration-Rotation Spectra*; Elsevier: Amsterdam, 1982.
[56] Martin, J. M. L.; Taylor, P. R. Accurate *ab Initio* Quartic Force Field for *trans*-HNNH and Treatment of Resonance Polyads. *Spectrochim. Acta A* **1997**, *53*, 1039–1050.
[57] Becke, A. D. Density-Functional Thermochemistry. III. The Role of Exact Exchange. *J. Chem. Phys.* **1993**, *98*, 5648–5652.
[58] Yang, W. T.; Parr, R. G.; Lee, C. T. Various Functionals for the Kinetic Energy Density of an Atom or Molecule. *Phys. Rev. A* **1986**, *34*, 4586–4590.
[59] Lee, C.; Yang, W. T.; Parr, R. G. Development of the Colle-Salvetti Correlation-Energy Formula into a Functional of the Electron Density. *Phys. Rev. B.* **1988**, *37*, 785–789.
[60] Dunning, T. H. Gaussian Basis Sets for Use in Correlated Molecular Calculations. I. The Atoms Boron through Neon and Hydrogen. *J. Chem. Phys.* **1989**, *90*, 1007–1023.
[61] Frisch, M. J. et al. Gaussian 09 Revision D.01. 2009; Gaussian Inc. Wallingford CT.
[62] Yu, Q.; Bowman, J. M.; Fortenberry, R. C.; Mancini, J. S.; Lee, T. J.; Crawford, T. D.; Klemperer, W.; Francisco, J. S. The Structure, Anharmonic Vibrational Frequencies, and Intensities of $NNHNN^+$. *J. Phys. Chem. A* **2015**, *119*, 11623–11631.
[63] Finney, B.; Fortenberry, R. C.; Francisco, J. S.; Peterson, K. A. A Spectroscopic Case for SPSi Detection: The Third-Row in a Single Molecule. *J. Chem. Phys.* **2016**, *145*, 124311.
[64] Molster, F. J.; Lim, T. L.; Sylvester, R. J.; Waters, L. B. F. M.; Barlow, M. J.; Beintema, D. A.; Cohen, M.; Cox, P.; Schmitt, B. The Complete ISO Spectrum of NGC 6302. *Astron. Astrophys.* **2001**, *372*, 165–172.

CHAPTER III: ROTATIONAL CONSTANTS

Reprinted from [21]

Gardner, M. B.; Westbrook, B. R.; Fortenberry, R. C.; Lee, T. J. Highly-Accurate Quartic Force Fields for the Prediction of Anharmonic Rotational Constants and Fundamental Vibrational Frequencies. *Spectrochimica Acta Part A: Molecular and Biomolecular Spectroscopy* 2021, *248*, 119184.

Highly-Accurate Quartic Force Fields for the Prediction of Anharmonic Rotational Constants and Fundamental Vibrational Frequencies

Mason B. Gardner

Department of Chemistry & Biochemistry, University of Mississippi, University, MS 38677-1848

Brent R. Westbrook

Department of Chemistry & Biochemistry, University of Mississippi, University, MS 38677-1848

Ryan C. Fortenberry

Department of Chemistry & Biochemistry, University of Mississippi, University, MS 38677-1848

Timothy J. Lee

MS 245-3, NASA Ames Research Center, Moffett Field, CA 94035

Abstract

The CcCR quartic force field (QFF) methodology is capable of computing B_0 and C_0 rotational constants to within 35 MHz (0.14%) of experiment for triatomic and larger molecules with at least two heavy atoms. Additionally, the same constants for molecules with four or more atoms agree to within 20 MHz (0.12%) of experiment for the current test set. This work also supports previous claims that the same QFF methodology can produce fundamental vibrational frequencies with a deviation less than 5.7 cm^{-1} from experiment. Consequently, this approach of augmenting complete basis set extrapolated energies with treatments of core electron correlation and scalar relativity produces some of the most accurate rovibrational spectroscopic data available.

Keywords: Quantum Chemistry; Quartic Force Fields; Rotational Spectroscopy; Vibrational Spectroscopy; Coupled Cluster Theory

1. Introduction

Quartic force fields (QFFs) making use of coupled cluster theory, specifically at the singles, doubles, and perturbative triples [CCSD(T)] level of theory [1], and other post-CCSD(T) effects have been shown to produce exceptionally accurate vibrational frequencies and rotational constants [2, 3]. These accuracies are reported to be within 1.0 cm^{-1}

Email address: r410@olemiss.edu (Ryan C. Fortenberry)

on occasion and often within 5.0 cm^{-1} of gas-phase experiment for vibrational frequencies, and within 30 or so MHz for the B and C rotational constants [4–15]. While these anecdotal values are promising for the composite method employed, a more systematic analysis of how the QFF performs for the prediction of these observable spectroscopic values is necessary.

The above-mentioned accurate QFF employs CCSD(T) in a complete basis set (CBS) extrapolation scheme [16] utilizing the aug-cc-pVTZ, aug-cc-pVQZ, and aug-cc-pV5Z basis sets [17–19, 16, 20]. The difference in the CCSD(T) energy with and without the inclusion of core electrons is used to correct the CBS energy for the effects of core correlation. These computations most often utilize the Martin-Taylor (MT) core electron basis set [21], but the more standard aug-cc-pCVTZ basis set has been shown to be just as viable [4, 22, 23]. Additional corrections for scalar relativity are incorporated using the Douglas-Kroll (DK) Hamiltonian [24, 25] by taking the difference in the CCSD(T)/cc-pVTZ-DK energies including and excluding the relativisitic terms. This use of the CCSD(T)/CBS energy ("C") including corrections for core correlation ("cC") and scalar relativity ("R") is often called the CcCR QFF [26]. Additional corrections for higher-order electron correlation ("E") and even quantum electrodynamics ("Q") can be added for presumed higher accuracy. For most molecules, save for those with higher bond orders, such terms do not improve the accuracy of the computations for molecules containing third-row or smaller atoms by more than 1.0 cm^{-1} in many cases but increase the computational cost of the QFF by more than a factor of 2, especially if higher-order coupled cluster truncations beyond full triples are included [4, 6, 26, 23].

Consequently, the CcCR QFF has been touted as a sweetspot for accuracy and computational cost in the determination of anharmonic vibrational frequencies and rotational constants. While errors in vibrational fundamentals have rarely reached above 10 cm^{-1} for the CcCR QFF, some cases have arisen where the rotational constants are in error by more than 100 MHz [4, 5]. As such, the present work will analyze a set of small molecules for which there are known, highly-accurate experimental data available for comparison to computed CcCR QFF rotational constants. Some vibrational frequencies will also be characterized as a part of this study, but rotational constants remain the principle focus. Other groups have established various means of computing quantum chemical rotational constants with much success even aiding in the detection of new molecules in space via radiotelescopes [27–34]. However, the present work will focus solely on the CcCR approach.

In particular, less computationally intensive perturbation theory (PT) approaches exist for obtaining highly-accurate rotational constants within 0.05% of gas-phase experimental values [35, 36]. The level of theory required for accurate vibrational corrections to equilibrium rotational constants is also quite low, with even B3LYP [37–39] offering reasonable accuracy for well-behaved systems [40]. However, these previous results rely on fortuitous characteristics of the systems investigated, primarily molecules composed of hydrogen, carbon, nitrogen, and oxygen. CcCR, on the other hand, is a more rigorous theoretical technique that is applicable to broader classes of molecules. Additionally, the CcCR methodology uses composite energies to make up the force field rather than correcting the observables afterwards. Previous work has clearly demonstrated the reliability of CcCR fundamental frequencies [3], but the goal of the present study is to analyze its efficacy in the computation of rotational constants. Such constants are often produced as a byproduct of a given vibrational study, so a better understanding of

their typical accuracy is needed to accompany future CcCR investigations and to further contextualize previous ones.

Variational approaches to the determination of rotational data also exist [41, 42], but these are typically much more costly, raising issues as to whether the additional cost is worth the accuracy gains [3]. Again, the focus here is on assessing the established CcCR/PT approach, not reviewing theoretical rovibrational spectroscopic techniques. With this in mind, the selection of molecules has been drawn from the CcCR/PT literature rather than from a broader pool of computed spectra. The literature selection is further augmented by new work on HCN, HCO^+, HNC, HMgNC, HNO, NH_3, H_2CO, and HOCN, which helps to tease out trends in the existing data. To further limit the scope of the present work, all of the molecules studied herein are covalently bound. More weakly-bound structures lead to very flat potential energy surfaces, which are poorly treated by QFFs in general [43, 44], especially those relying upon numerical differentiation. Thus, the present work will serve to benchmark the performance of the CcCR/PT QFF for various classes of small (3-6 atoms), covalent molecules, for which accurate gas-phase experimental rotational data are available.

2. Computational Details

The computation of CcCR QFFs begins with geometry optimizations of the desired molecule via CCSD(T)/aug-cc-pV5Z. The geometry is then corrected for changes resulting from differences in CCSD(T)/MT optimizations with and without core electrons included. These reference geometries are then displaced by 0.005 Å and 0.005 radians per each step per each symmetry-internal coordinate. The QFF is of the form:

$$V = \frac{1}{2}\sum_{ij} F_{ij}\Delta_i\Delta_j + \frac{1}{6}\sum_{ijk} F_{ijk}\Delta_i\Delta_j\Delta_k + \frac{1}{24}\sum_{ijkl} F_{ijkl}\Delta_i\Delta_j\Delta_k\Delta_l, \tag{1}$$

where the $F_{ij\ldots}$ terms are the force constants and the $\Delta_i\Delta_j\ldots$ terms are the displaced distances for coordinates i, j, and so forth [45, 46]. Then, at each point ($\Delta_i\Delta_j\ldots$), the seven energies necessary for the CcCR QFF are computed. These are then fit via a least-squares procedure and refit in order to produce zero gradients, the resulting equilibrium geometry, and the other force constants ($F_{ij\ldots}$) for the potential function in Equation 1 [4, 6].

The force constants are then transformed into generic Cartesian coordinates for general usage through the INTDER2005 program [47]. The Cartesian force constants are utilized in the SPECTRO program [48] to produce the rotational constants and anharmonic vibrational frequencies. Coriolis and Fermi resonances, as well as Fermi resonance polyads [49], are then included in the second-order perturbation theory [50–52] treatment of the vibrational and rotational Hamiltonians within SPECTRO in order to produce the most accurate spectroscopic data possible within a perturbation theory approach.

Once the CcCR QFF data are determined for the present work, these are compared with experimental data taken from the chemical literature. Other, theoretical CcCR rotational constants and fundamental vibrational frequencies are taken from the literature, as well, in order to provide a larger data set. For the present work, most of the molecules explored are closed-shell, but some are radicals providing a breadth of molecules. The full list is given in Tables 1 and 2. In all cases, the experimental rotational constants

and fundamental vibrational frequencies are subtracted from the computed CcCR QFF second-order perturbation theory values to yield the reported differences. The absolute values of these differences are averaged herein in order to produce the mean absolute error or MAE. The percent error is calculated, using

$$\frac{|\text{Diff.}|}{\text{Experiment}} \times 100\%, \tag{2}$$

where |Diff.| is the absolute value of the aforementioned difference. The rotational constants are also divided into subgroups in order to tease out the behavior of certain types of molecules with certain properties or characteristics. In addition to MAEs for these groups, the mean absolute percent errors (MA%Es) are reported in Table 3.

3. Results and Discussion

The CcCR quartic force field approach provides exceptional accuracy in the prediction of vibrationally-averaged rotational constants in most cases. The full set of principle rotational constants considered in this work is given in Table 1. The sources of the data are listed in Table 2 with eight CcCR molecular datasets original to this work: HCN, HCO^+, HNC, HMgNC, HNO, NH_3, H_2CO, and HOCN. Clearly from Table 1, many systems have excellent correspondence between CcCR QFF theory and gas-phase experiment while some are less accurate. The MAE for the entire set of rotational constants is 537.4 MHz (0.20%) as listed in Table 3. Most evidently, the A_0 rotational constants vary by significantly greater amounts than B_0 and C_0, both in terms of absolute errors and even for the percent errors. Many of the molecules in this set are near-prolate, and the larger magnitude of the A constant contributes to this difference. Besides the oblate c-$C_3H_3{}^+$, the least prolate molecule, c-C_3H_2, has the smallest error for the CcCR QFF A_0 compared to experiment at 64.0 MHz. Such behavior in near-prolate molecules is known within the quantum chemistry community [27, 28], and this is borne out in the MAE for the A constants alone at 1577.5 MHz (0.31%).

However, such a large error incorrectly implies that CcCR QFF computations are insufficient for predicting spectroscopic constants. Removing the A constants from consideration certainly improves the average rotational constant and also even lowers the percent error. Linear molecules have degenerate B and C constants, and averaging over B_0 and C_0 requires counting the B constant in the linear molecules twice. Such an average of B_0 and C_0 with A_0 removed reduces the MAE by an order of magnitude to 92.7 MHz (0.15%) in line two of Table 3.

Closer inspection of Table 1 shows that several molecules appear to be outliers with absolute errors for B_0 and C_0 in the range of 100+ MHz. Most of these are hydrides with a lone heavy atom: $NH_2{}^-$, H_2O, and NH_3. Removing the rotational constant errors for these three molecules lowers the MAE by roughly one-third to 34.6 MHz (0.14%).

The error in the computed versus experimental rotational constants of water has been known since the formulation of the CcCR family of composite QFF schema [4], and this work shows that such simple systems are often the most difficult to model. The reason for this poor behavior in light molecules is multifaceted. First, these molecules have larger rotational constants implying that regular percent errors manifest themselves with higher magnitude differences from experiment. Second, these molecules have large

Table 1: The CcCR Equilibrium & Vibrationally-Averaged and Gas Phase Experimental Rotational Constants in MHz.

		CcCR					
Molecule		Equil.	Vib. Avg.	Experiment	Difference	|Diff.|	% Error
HCN	B	44580.6	44386.4	44316	70.4	70.4	0.16
HCO^+	B	44851.4	44611.1	44594.4	16.7	16.7	0.04
HNC	B	45571.5	45405.3	45332	73.3	73.3	0.16
C_2H	B	44187.6	43702.2	43674.5	27.7	27.7	0.06
C_2H^-	B	41735.7	41568.7	41639.2	−70.5	70.5	0.17
HMgNC	B	5436.4	5471.0	5481.4	−10.4	10.4	0.19
$NH_2{}^-$	A	688371.4	689654.6	691045.6	−1391.0	1391.0	0.20
	B	392881.0	391702.8	391780.8	−78.0	78.0	0.02
	C	250125.8	243476.4	243269.6	206.8	206.8	0.09
H_2O	A	820382.1	831542.7	835840.3	−4297.6	4297.6	0.51
	B	438356.5	436042.4	435351.7	690.7	690.7	0.16
	C	285702.2	278664.6	278138.7	525.9	525.9	0.19
HNO	A	566875.5	560818.2	553898.6	6919.6	6919.6	1.25
	B	42534.6	42430.6	42312.8	117.8	117.8	0.28
	C	39566.0	39281.6	39165.1	116.5	116.5	0.30
HSO	A	302261.2	300113.4	299483.9	629.5	629.5	0.21
	B	20715.7	20597.8	20502.8	95.0	95.0	0.46
	C	19387.0	19219.9	19135.7	84.2	84.2	0.44
HSS	A	299200.8	297770.1	296974.4	795.7	795.7	0.27
	B	8030.6	8009.9	7996.4	13.5	13.5	0.17
	C	7820.7	7790.4	7776.7	13.7	13.7	0.18
HPSi	A	306054.4	296974.9	297187	−212.1	212.1	0.07
	B	8211.2	8169.4	8169	0.4	0.4	0.00
	C	7996.6	7939.1	7936.7	2.4	2.4	0.03
SiC_2	A	52343.2	52602.5	52473.7	128.8	128.8	0.25
	B	13264.2	13145.8	13158.7	−12.8	12.8	0.10
	C	10582.5	10444.8	10442.6	2.1	2.1	0.02
NH_3	A	299988.5	297539.8	298107	−567.2	567.2	0.19
	C	190683.3	186445.2	185751.4	693.8	693.8	0.37
H_2CO	A	285857.2	282684.0	281963.8	720.2	720.2	0.26
	B	39055.5	38898.6	38832.1	66.5	66.5	0.17
	C	34361.0	34058.7	34002.5	56.2	56.2	0.17
HOCN	A	673758.4	677180.7	674308	2872.7	2872.7	0.43
	B	10622.2	10592.4	10577	15.4	15.4	0.15
	C	10457.4	10414.3	10398	16.3	16.3	0.16
cis-HOCO	A	141896.9	143151.8	142944.9	206.9	206.9	0.14
	B	11856.5	11757.3	11739.6	17.7	17.7	0.15
	C	10942.1	10846.5	10830	16.5	16.5	0.15
trans-HOCO	A	167470.4	168266.3	167768.1	498.2	498.2	0.30
	B	11535.7	11448.5	11433.2	15.3	15.3	0.13
	C	10792.5	10702.0	10686.7	15.3	15.3	0.14
$HOCO^+$	A	765443.3	784759.5	789951	−5191.5	5191.5	0.66
	B	10818.6	10787.1	10773.6	13.5	13.5	0.13
	C	10667.2	10623.7	10609.4	14.3	14.3	0.13
$NNOH^+$	A	624453.7	625221.3	625957.716	−736.4	736.4	0.12
	B	11357.9	11306.9	11301.5628	5.3	5.3	0.05
	C	11155.0	11090.2	11084.28	6.0	6.0	0.05
c-C_3H_2	A	35377.2	35156.6	35092.6	64.0	64.0	0.18
	B	32420.0	32243.1	32212.9	30.2	30.2	0.09
	C	16917.1	16767.7	16749.3	18.4	18.4	0.11
c-$C_3H_3{}^+$	A	30956.6	30761.7	30753.9	7.8	7.8	0.03
	B	30956.6	30761.7	30753.9	7.8	7.8	0.03
	C	15478.3	15342.8	15338.9	3.9	3.9	0.03
Average					63.1	537.4	0.20

Table 2: The CcCR and Gas Phase Experimental References.

Molecule	CcCR	Experiment
HCN	This Work	53
HCO^+	This Work	54–59
HNC	This Work	60, 61
C_2H	62	63–66
C_2H^-	5	67, 68
HMgNC	This Work	69
$NH_2{}^-$	5	70
H_2O	4	71
HNO	This Work	72
HSO	73	74, 31
HSS	73	75
HPSi	76	27
SiC_2	11	77, 78
NH_3	This Work	79, 80
H_2CO	This Work	80
HOCN	This Work	81, 82
cis-HOCO	83	84
trans-HOCO	26	84
$HOCO^+$	8	85
$NNOH^+$	9	86, 87
c-C_3H_2	15	88
c-$C_3H_3{}^+$	6	7

Table 3: Average Errors for CcCR vs. Experiment for Various Cases.

Set	Units	MAE	MA%E
A_0, B_0, & C_0	MHz	537.4	0.20
B_0 & C_0	MHz	92.7	0.15
B_0 & C_0 w/o H_2O, $NH_2{}^-$, & NH_3	MHz	34.6	0.14
B_0 & C_0 w/o Triatomics & NH_3	MHz	18.9	0.12
A_0	MHz	1577.5	0.32
ν_x	cm^{-1}	5.7	0.70

anharmoniciites, as well. This shifts the zero-point structure and, subsequently, the rotational constants by more than is typical for treatment from second-order rotational perturbation theory. A large anharmonicity is also present in HNO which is known to have an extreme anharmonicity for the N−H stretch [89]. Here the B_0 and C_0 are in error from experiment by 117.8 MHz and 116.5 MHz, respectively, marking the largest deviations for molecules in this set with at least two heavy atoms. This is also borne out in the percent errors for this molecule which are the largest for both sets inclusive and exclusive of A. Formaldehyde is roughly the same mass as HNO and also has relatively large errors for B_0 and C_0, but these are roughly half the magnitude and percent error of that in HNO. Hence, the anharmonicity and large rotational constants present in the three single-heavy-atom hydrides are driving this error beyond that of molecules containing multiple heavy atoms.

Further constraining the data set by removing all of the triatomic species and ammonia produces an MAE of only 18.9 MHz (0.12%). The increase in mass and decrease in the rotational constant values continue to drive the error down for the comparison between theory and experiment. The nine molecules remaining in the present set range in shape from linear to oblate. They contain standard p-block elements, in addition to Mg, and consist of both open- and closed-shell molecules. Formaldehyde has the largest errors of 66.5 MHz and 56.2 MHz while the next largest come from c-C_3H_2 at 30.2 MHz and 18.4 MHz. Save for HMgNC, all of the computed rotational constants are larger than their experimental counterparts. Consequently, the CcCR VPT2 QFF B_0 and C_0 rotational constants can be said to be within 20 MHz or 0.12% of experiment for four-atom and larger molecular systems. Such accuracy should be sufficient for comparison with high-resolution gas-phase experiment and potentially even radioastronomical observation.

Since QFFs have been utilized to compute the rotational constants from CcCR, fundamental vibrational frequencies are also produced in this methodology. Consequently, the present work provides a novel means for analyzing the performance of CcCR QFF second-order vibrational perturbation theory (VPT2) in predicting fundamental vibrational frequencies. Fewer molecules of our sample set have gas-phase, experimental vibrational spectral data available, but 12 molecules have at least one high-resolution experimentally known, gas-phase fundamental vibrational frequency giving 36 frequencies for comparison as given in Table 4. For this set, the MAE per fundamental is 5.7 cm^{-1}. Consequently, the typical error reported previously for the CcCR QFF VPT2 fundamental vibrational frequencies as mentioned in the introduction is verified for a larger set of molecules. Furthermore, of the 36 frequencies contained in this set, only one has an error of greater than 15 cm^{-1} (SiC_2 at 21.0 cm^{-1}), and 23 are less than 5 cm^{-1} with errors for seven fundamentals of less than 2 cm^{-1}.

4. Conclusions

Quantum chemically-computed rotational constants are accurately represented from CcCR QFFs provided that the molecules of interest contain more than two heavy atoms. The MAE for the B_0 and C_0 constants for our set of explored molecules is 34.6 MHz (0.14%) when the smallest hydrides are excluded. Larger ($\geq$ 4 atoms) and less anharmonic molecules have an even better MAE at 18.9 MHz (0.12%). The smallest B_0 and C_0 errors from our set are from the relatively massive HPSi molecule (0.4 MHz and 2.4

Table 4: The CcCR and Gas Phase Experimental Fundamental Vibrational Frequencies in cm^{-1}.

Molecule		CcCR	Experiment	Difference	|Diff.|	% Error
HCN	ν_1	3313.1	3311.47	1.6	1.6	0.05
	ν_2	719.7	711.97	7.7	7.7	0.45
	ν_3	2106.2	2096.84	9.3	9.3	1.09
HCO^+	ν_1	3089.8	3088.73951	1.0	1.0	0.03
	ν_2	2189.9	2183.94961	6.0	6.0	0.27
	ν_3	833.4	829.72	3.7	3.7	0.44
HNC	ν_1	3655.0	3652.65	2.3	2.3	0.06
	ν_2	2027.7	2023.86	3.8	3.8	0.19
	ν_3	474.8	462.72	12.1	12.1	2.61
H_2O	ν_1	3659.7	3657.05	2.7	2.7	0.07
	ν_2	1595.8	1597.75	−1.9	1.9	0.12
	ν_3	3758.0	3755.93	2.1	2.1	0.06
HNO	ν_1	2688.8	2684	4.8	4.8	0.18
	ν_2	1577.1	1565	12.1	12.1	0.77
	ν_3	1510.8	1501	9.8	9.8	0.65
SiC_2	ν_1	1750.5	1746.0	4.5	4.5	0.26
	ν_2	844.7	840.6	4.1	4.1	0.49
	ν_3	175.4	196.37	−21.0	21.0	0.68
NH_3	ν_1	3445.5	3444	1.5	1.5	0.04
	ν_2	3346.0	3337	9.0	9.0	0.27
	ν_3	1628.7	1627	1.7	1.7	0.10
	ν_4	974.2	950	24.2	24.2	2.55
H_2CO	ν_1	2832.6	2843	−10.4	10.4	0.37
	ν_2	2782.5	2782	0.5	0.5	0.02
	ν_3	1751.1	1746	5.1	5.1	0.29
	ν_4	1501.8	1500	1.8	1.8	0.12
	ν_5	1251.0	1249	2.0	2.0	0.16
	ν_6	1171.5	1167	4.5	4.5	0.39
HOCN	ν_1	3623.0	3610	13.0	13.0	0.36
	ν_2	2298.5	2302	−3.5	3.5	0.15
	ν_3	1231.3	1227	4.3	4.3	0.35
	ν_4	1087.4	1082	5.4	5.4	0.50
	ν_6	454.6	460	−5.4	5.4	1.17
$HOCO^+$	ν_1	3371.2	3375.37413	−4.2	4.2	0.12
$NNOH^+$	ν_1	3332.0	3330.91	1.1	1.1	0.03
c-C_3H_2	ν_4	1278.8	1278.8	0.0	0.0	0.00
	ν_5	1065.1	1061.5	3.6	3.6	0.34
	ν_7	888.6	886.4	2.2	2.2	0.25
	ν_9	772.8	787.4	−14.6	14.6	1.85
c-$C_3H_3{}^+$	ν_4	3131.7	3131.1447	0.6	0.6	0.02
Average				2.7	5.7	0.70

MHz); the next smallest are for c-$C_3H_3^+$ at 7.8 MHz and 3.9 MHz implying that the CcCR approach is largely agnostic to atom type at this point. The largest of the well-behaved set are for formaldehyde at 66.5 MHz and 56.2 MHz, but most are less than 20 MHz, roughly the MAE. Such accuracies are close to the limits that can be utilized for direct astronomical observation. While a forest of lines are present in any spectral window observed towards interesting astronomical objects, the CcCR QFF theoretical rotational spectral progressions will be shifted only slightly when compared to such observations.

Additionally, the CcCR QFF is benchmarked to predict fundamental vibrational frequencies to within 5.7 cm^{-1}, further showcasing the accuracy of this method in use for the past decade or so. While CCSD(T)-F12/cc-pVTZ-F12 has been shown to mirror the accuracies of the CcCR composite QFF in computing vibrational frequencies [90, 91], explicitly correlated theory cannot provide the same relative errors for the rotational constants. While composite schema for explicitly correlated methods may yet produce more accurate rotational constants [92], the canonical-CCSD(T)-based CcCR QFF remains one of the most accurate approaches for computing rotational constants developed thus far.

5. Acknowledgements

This work by the Unviersity of Mississippi (UM) group has been supported by NASA Grant NNX17AH15G, NSF Grant OIA-1757220, and start-up funds provided by UM. TJL gratefully acknowledge financial support from the 17-APRA17-0051, 18-APRA18-0013, and 18-2XRP18_2-0046 NASA grants.

References

[1] Raghavachari, K.; Trucks, G. W.; Pople, J. A.; Replogle, E. Highly Correlated Systems: Structure, Binding Energy and Harmonic Vibrational Frequencies of Ozone. *Chem. Phys. Lett.* **1989**, *158*, 207–212.

[2] Császár, A. G. Anharmonic Molecular Force Fields. *WIREs Comput. Mol. Sci.* **2012**, *2*, 273–289.

[3] Fortenberry, R. C.; Lee, T. J. Computational Vibrational Spectroscopy for the Detection of Molecules in Space. *Ann. Rep. Comput. Chem.* **2019**, *15*, 173–202.

[4] Huang, X.; Lee, T. J. A Procedure for Computing Accurate *Ab Initio* Quartic Force Fields: Application to HO_2^+ and H_2O. *J. Chem. Phys.* **2008**, *129*, 044312.

[5] Huang, X.; Lee, T. J. Accurate *Ab Initio* Quartic Force Fields for NH_2^- and CCH^- and Rovibrational Spectroscopic Constants for Their Isotopologs. *J. Chem. Phys.* **2009**, *131*, 104301.

[6] Huang, X.; Taylor, P. R.; Lee, T. J. Highly Accurate Quartic Force Field, Vibrational Frequencies, and Spectroscopic Constants for Cyclic and Linear $C_3H_3^+$. *J. Phys. Chem. A* **2011**, *115*, 5005–5016.

[7] Zhao, D.; Doney, K. D.; Linnartz, H. Laboratory Gas-Phase Detection of the Cyclopropenyl Cation (c-$C_3H_3^+$). *Astrophys. J. Lett.* **2014**, *791*, L28.

[8] Fortenberry, R. C.; Huang, X.; Francisco, J. S.; Crawford, T. D.; Lee, T. J. Quartic Force Field Predictions of the Fundamental Vibrational Frequencies and Spectroscopic Constants of the Cations $HOCO^+$ and $DOCO^+$. *J. Chem. Phys.* **2012**, *136*, 234309.

[9] Huang, X.; Fortenberry, R. C.; Lee, T. J. Protonated Nitrous Oxide, $NNOH^+$: Fundamental Vibrational Frequencies and Spectroscopic Constants from Quartic Force Fields. *J. Chem. Phys.* **2013**, *139*, 084313.

[10] Fortenberry, R. C.; Huang, X.; Crawford, T. D.; Lee, T. J. Quartic Force Field Rovibrational Analysis of Protonated Acetylene, $C_2H_3^+$, and Its Isotopologues. *J. Phys. Chem. A* **2014**, *118*, 7034–7043.

[11] Fortenberry, R. C.; Lee, T. J.; Müller, H. S. P. Excited Vibrational Level Rotational Constants for SiC_2: A Sensitive Molecular Diagnostic for Astrophysical Conditions. *Molec. Astrophys.* **2015**, *1*, 13–19.

[12] Kitchens, M. J. R.; Fortenberry, R. C. The Rovibrational Nature of Closed-Shell Third-Row Triatomics: HOX and HXO, X = Si^+, P, S^+, and Cl. *Chem. Phys.* **2016**, *472*, 119–127.

[13] Bizzocchi, L.; Lattanzi, V.; Laas, J.; Spezzano, S.; Giuliano, B. M.; Prudenzano, D.; Endres, C.; Sipilä, O.; Caselli, P. Accurate Sub-millimetre Rest Frequencies for $HOCO^+$ and $DOCO^+$ Ions. *Astron. Astrophys.* **2017**, *602*, A34.

[14] Fortenberry, R. C. Quantum Astrochemical Spectroscopy. *Int. J. Quant. Chem.* **2017**, *117*, 81–91.

[15] Fortenberry, R. C.; Novak, C. M.; Layfield, J. P.; Matito, E.; Lee, T. J. Overcoming the Failure of Correlation for Out-of-Plane Motions in a Simple Aromatic: Rovibrational Quantum Chemical Analysis of *c*-C_3H_2. *J. Chem. Theor. Comput.* **2018**, *14*, 2155–2164.

[16] Martin, J. M. L.; Lee, T. J. The Atomization Energy and Proton Affinity of NH_3. An *Ab Initio* Calibration Study. *Chem. Phys. Lett.* **1996**, *258*, 136–143.

[17] Dunning, T. H. Gaussian Basis Sets for Use in Correlated Molecular Calculations. I. The Atoms Boron through Neon and Hydrogen. *J. Chem. Phys.* **1989**, *90*, 1007–1023.

[18] Kendall, R. A.; Dunning, T. H.; Harrison, R. J. Electron Affinities of the First-Row Atoms Revisited. Systematic Basis Sets and Wave Functions. *J. Chem. Phys.* **1992**, *96*, 6796–6806.

[19] Peterson, K. A.; Dunning, T. H. Benchmark Calculations with Correlated Molecular Wave Functions. VII. Binding Energy and Structure of the HF Dimer. *J. Chem. Phys.* **1995**, *102*, 2032–2041.

[20] Fortenberry, R. C.; Huang, X.; Francisco, J. S.; Crawford, T. D.; Lee, T. J. Fundamental Vibrational Frequencies and Spectroscopic Constants of $HOCS^+$, $HSCO^+$, and Isotopologues via Quartic Force Fields. *J. Phys. Chem. A.* **2012**, *116*, 9582–9590.

[21] Martin, J. M. L.; Taylor, P. R. Basis Set Convergence for Geometry and Harmonic Frequencies. Are *h* Functions Enough? *Chem. Phys. Lett.* **1994**, *225*, 473–479.

[22] Fortenberry, R. C.; Huang, X.; Crawford, T. D.; Lee, T. J. The 1 $^3A'$ HCN and 1 $^3A'$ HCO^+ Vibrational Frequencies and Spectroscopic Constants from Quartic Force Fields. *J. Phys. Chem. A.* **2013**, *117*, 9324–9330.

[23] Cheng, Q.; Fortenberry, R. C.; DeYonker, N. J. Towards a Quantum Chemical Protocol for the Prediction of Rovibrational Spectroscopic Data for Transition Metal Molecules: Exploration of CuCN, CuOH, and CuCCH. *J. Chem. Phys.* **2017**, *147*, 234303.

[24] Douglas, M.; Kroll, N. Quantum Electrodynamical Corrections to the Fine Structure of Helium. *Ann. Phys.* **1974**, *82*, 89–155.

[25] Jansen, G.; Hess, B. A. Revision of the Douglas-Kroll Hamiltonian. *Phys. Rev. A* **1989**, *39*, 6016–6017.

[26] Fortenberry, R. C.; Huang, X.; Francisco, J. S.; Crawford, T. D.; Lee, T. J. The *trans*-HOCO Radical: Fundamental Vibrational Frequencies, Quartic Force Fields, and Spectroscopic constants. *J. Chem. Phys.* **2011**, *135*, 134301.

[27] Lattanzi, V.; Thorwirth, S.; Halfen, D. T.; Mück, L. A.; Ziurys, L. M.; Thaddeus, P.; Gauss, J.; McCarthy, M. C. Bonding in the Heavy Analogue of Hydrogen Cyanide: The Curious Case of Bridged HPSi. *Angew. Chem. Int. Ed. Engl.* **2010**, *49*, 5661–5664.

[28] Barone, V.; Biczysko, M.; Puzzarini, C. Quantum Chemistry Meets Spectroscopy for Astrochemistry: Increasing Complexity toward Prebiotic Molecules. *Acc. Chem. Res.* **2015**, *48*, 1413–1422.

[29] Cernicharo, J.; McCarthy, M. C.; Gottlieb, C. A.; Agúndez, M.; Prieto, L. V.; Baraban, J. H.; Changala, P. B.; Guéein, M.; Kahane, C.; Martin-Drumel, M. A.; Patel, N. A.; Reilly, N. J.; Stanton, J. F.; Quintana-Lacaci, G.; Thorwirth, S. Discovery of SiCSi in IRC+10216: A Missing Link between Gas and Dust Carriers of Si-C Bonds. *Astrophys. J. Lett.* **2015**, *806*, L3.

[30] McCarthy, M. C.; Baraban, J. H.; Changala, P. B.; Stanton, J. F.; Martin-Drumel, M.-A.; Thorwirth, S.; Gottlieb, C. A.; Reilly, N. J. Discovery of a Missing Link: Detection and Structure of the Elusive Disilicon Carbide Cluster. *J. Phys. Chem. Lett.* **2015**, *6*, 2107–2111.

[31] Cazzoli, G.; Lattanzi, V.; Kirsch, T.; Gauss, J.; Belén Tercero and, J. C.; Puzzarini, C. Laboratory Measurements and Astronomical Search for the HSO Radical. *Astron. Astrophys.* **2016**, *591*, A126.

[32] Finney, B.; Fortenberry, R. C.; Francisco, J. S.; Peterson, K. A. A Spectroscopic Case for SPSi Detection: The Third-Row in a Single Molecule. *J. Chem. Phys.* **2016**, *145*, 124311.

[33] Demaison, J.; Craig, N. C.; Gurusinghe, R.; Tubergen, M. J.; Rudolph, H. D.; Coudert, L. H.; Szalay, P. G.; Császár, A. G. Fourier Transform Microwave Spectrum of Propene-3-d_1 (CH_2 =$CHCH_2D$), Quadrupole Coupling Constants of Deuterium, and a Semiexperimental Equilibrium Structure of Propene. *J. Phys. Chem. A* **2017**, *121*, 3155–3166.

[34] Puzzarini, C.; Barone, V. Diving for Accurate Structures in the Ocean of Molecular Systems with

the Help of Spectroscopy and Quantum Chemistry. *Acc. Chem. Res.* **2018**, *51*, 548–556.
[35] Puzzarini, C.; Heckert, M.; Gauss, J. The Accuracy of Rotational Constants Predicted by High-Level Quantum-Chemical Calculations. I. Molecules Containing First-Row Atoms. *J. Chem. Phys.* **2008**, *128*, 194108.
[36] Alessandrini, S.; Gauss, J.; Puzzarini, C. Accuracy of Rotational Parameters Predicted by High-Level Quantum-Chemical Calculations: Case Study of Sulfur-Containing Molecules of Astrochemical Interest. *J. Chem. Theory Comput* **2018**, *14*, 5360–5371.
[37] Yang, W. T.; Parr, R. G.; Lee, C. T. Various Functionals for the Kinetic Energy Density of an Atom or Molecule. *Phys. Rev. A* **1986**, *34*, 4586–4590.
[38] Lee, C.; Yang, W. T.; Parr, R. G. Development of the Colle-Salvetti Correlation-Energy Formula into a Functional of the Electron Density. *Phys. Rev. B.* **1988**, *37*, 785–789.
[39] Becke, A. D. Density-Functional Thermochemistry. III. The Role of Exact Exchange. *J. Chem. Phys.* **1993**, *98*, 5648–5652.
[40] Piccardo, M.; Penocchio, E.; Puzzarini, C.; Biczysko, M.; Barone, V. Semi-Experimental Equilibrium Structure Determinations by Employing B3LYP/SNSD Anharmonic Force Fields: Validation and Application to Semirigid Organic Molecules. *J. Phys. Chem. A* **2015**, *119*, 2058–2082.
[41] Carter, S.; Bowman, J. M.; Handy, N. C. Extensions and Tests of "Multimodes": a Code to Obtain Accurate Vibration/Rotation Energies of Many-Mode Molecules. *Theor. Chem. Acc.* **1998**, *100*, 191–198.
[42] Bowman, J. M.; Carter, S.; Huang, X. MULTIMODE: a Code to Calculate Rovibrational Energies of Polyatomic Molecules. *Int. Rev. Phys. Chem.* **2003**, *22*, 533–549.
[43] Yu, Q.; Bowman, J. M.; Fortenberry, R. C.; Mancini, J. S.; Lee, T. J.; Crawford, T. D.; Klemperer, W.; Francisco, J. S. The Structure, Anharmonic Vibrational Frequencies, and Intensities of $NNHNN^+$. *J. Phys. Chem. A* **2015**, *119*, 11623–11631.
[44] Bassett, M. K.; Fortenberry, R. C. Symmetry Breaking and Spectral Considerations of the Surprisingly Floppy *c*-C_3H Radical and the Related Dipole-Bound Excited State of *c*-C_3H^-. *J. Chem. Phys.* **2017**, *146*, 224303.
[45] Cramer, C. J. *Essentials of Computational Chemistry: Theories and Models*, 2nd ed.; Wiley: West Sussex, England, 2004.
[46] Lee, T. J.; Martin, J. M. L.; Taylor, P. R. An Accurate *ab Initio* Quartic Force Field and Vibrational Frequencies for CH_4 and Its Isotopomers. *J. Chem. Phys.* **1995**, *102*, 254–261.
[47] Allen, W. D.; coworkers, 2005; *INTDER* 2005 is a General Program Written by W. D. Allen and Coworkers, which Performs Vibrational Analysis and Higher-Order Non-Linear Transformations.
[48] Gaw, J. F.; Willets, A.; Green, W. H.; Handy, N. C. In *Advances in Molecular Vibrations and Collision Dynamics*; Bowman, J. M., Ratner, M. A., Eds.; JAI Press, Inc.: Greenwich, Connecticut, 1991; pp 170–185.
[49] Martin, J. M. L.; Taylor, P. R. Accurate *ab Initio* Quartic Force Field for *trans*-HNNH and Treatment of Resonance Polyads. *Spectrochim. Acta A* **1997**, *53*, 1039–1050.
[50] Mills, I. M. In *Molecular Spectroscopy - Modern Research*; Rao, K. N., Mathews, C. W., Eds.; Academic Press: New York, 1972; pp 115–140.
[51] Watson, J. K. G. In *Vibrational Spectra and Structure*; During, J. R., Ed.; Elsevier: Amsterdam, 1977; pp 1–89.
[52] Papousek, D.; Aliev, M. R. *Molecular Vibration-Rotation Spectra*; Elsevier: Amsterdam, 1982.
[53] Mellau, G. C. Complete experimental rovibrational eigenenergies of HCN up to 6880 cm^{-1} above the ground state. *J. Chem. Phys.* **2011**, *134*, 234303.
[54] Amano, T. The ν_1 Fundamental Band of HCO^+ by Difference Frequency Laser Spectroscopy. *J. Chem. Phys.* **1983**, *79*, 3595.
[55] Foster, S. C.; McKellar, A. R. W.; Sears, T. J. Observation of the ν_3 Fundamental Band of HCO^+. *J. Chem. Phys.* **1984**, *81*, 578.
[56] Davies, P. B.; Hamilton, P. A.; Rothwell, W. J. Infrared Laser Spectroscopy of the ν_3 Fundamental of HCO^+. *J. Chem. Phys.* **1984**, *81*, 1598–1599.
[57] Kawaguchi, K.; Yamada, C.; Saito, S.; Hirota, E. Magnetic Field Modulated Infrared Laser Spectroscopy of Molecular Ions: The ν_2 Band of HCO^+. *J. Chem. Phys.* **1985**, *82*, 1750–1755.
[58] Linnartz, H.; Speck, T.; Maier, J. P. High-Resolution Infrared Spectrum of the ν_3 Band in $Ar{-}HCO^+$. *Chem. Phys. Lett.* **1998**, *288*, 504–508.
[59] Cazzoli, G.; Cludi, L.; Buffa, G.; Puzzarini, C. Precise THz Measurements of HCO^+, N_2H^+, and CF^+ for Astrophysical Observations. *Astrophys. J. Suppl. Ser.* **2012**, *203*, 1–9.
[60] Mellau, G. C. The ν_1 band system of HNC. *J. Molec. Spectrosc.* **2010**, *264*, 2–9.
[61] Mellau, G. C. Complete experimental rovibrational eigenenergies of HNC up to 3743 cm^{-1} above

the ground state. *J. Chem. Phys.* **2010**, *133*, 164303.
[62] Morgan, W. J.; Fortenberry, R. C. Theoretical Rovibronic Treatment of the $\widetilde{X}\ ^2\Sigma^+$ and $\widetilde{A}\ ^2\Pi$ States of C_2H & $\widetilde{X}\ ^1\Sigma^+$ State of C_2H^- from Quartic Force Fields. *J. Phys. Chem. A* **2015**, *119*, 7013–7025.
[63] Stephens, J. W.; Yan, W.-B.; Richnow, M. L.; Solka, H.; Curl, R. F. Infrared Kinetic Spectroscopy of C_2H and C_2D. *J. Molec. Struct.* **1988**, *190*, 41–60.
[64] Endo, Y.; Kanamori, H.; Hirota, E. Millimeter- and Submillimeter-Wave Spectra of the Vibrationally Excited CCD Radical. *Chem. Phys. Lett.* **1987**, *160*, 280–284.
[65] Kanamori, H.; Seki, K.; Hirota, E. Infrared Diode Laser Kinetic Spectroscopy of the CCH Radical ν_3 Band. *J. Chem. Phys.* **1987**, *87*, 73–76.
[66] Kanamori, H.; Hirota, E. Vibronic Bands of the CCH Radical Observed by Infrared Diode Laser Kinetic Spectroscopy. *J. Chem. Phys.* **1988**, *88*, 3962–3969.
[67] Brünken, S.; Gupta, H.; Gottlieb, C. A.; McCarthy, M. C.; Thaddeus, P. Detection of the Carbon Chain Negative Ion C_8H^- in TMC-1. *Astrophys. J.* **2007**, *664*, L43–L46.
[68] Ervin, K.; Lineberger, W. C. Photoelectron Spectra of C_2 and C_2H^-. *J. Phys. Chem.* **1991**, *95*, 1167–1177.
[69] Cabezas, C.; Cernicharo, J.; Alonso, J. L.; Agúndez, M.; Mata, S.; Guélin, M.; Peña, I. Laboratory and Astronomical Discovery of Hydromagnesium Isocyanide. *Astrophys. J.* **2013**, *775*, 133.
[70] Tack, L. M.; Rosenbaum, N. H.; Owrutsky, J. C.; Saykally, R. J. Velocity Modulation Infrared Laser Spectroscopy and Structure of the Amide Anion ($NH_2{}^-$). *J. Chem. Phys.* **1986**, *85*, 4222–4227.
[71] Tennyson, J.; Zobov, N. F.; Williamson, R.; Polyansky, O. L. Experimental Energy Levels of the Water Molecule. *J. Phys. Chem. Ref. Data* **2001**, *30*, 735.
[72] Johns, J. W. C.; McKellar, A. R. W.; Weinberger, E. The Infrared Spectrum of HNO. *Canadian. J. Phys.* **1983**, *61*, 1106–1119.
[73] Fortenberry, R. C.; Francisco, J. S. On the Detectability of the $\tilde{X}^2A''$ HSS, HSO, and HOS Radicals in the Interstellar Medium. *Astrophys. J.* **2017**, *835*, 243.
[74] Yoshikawa, T.; Watanabe, A.; Sumiyoshi, Y.; Endo, Y. Laser Spectroscopy of the $\tilde{A}^2A' - \tilde{X}^2A''$ System for the HSO Radical. *J. Molec. Spectrosc.* **2009**, *254*, 119–125.
[75] Yamamoto, S.; Saito, S. Microwave Spectrum and Molecular Structure of the HS_2 Radical. *Can. J. Phys.* **1994**, *72*, 954–962.
[76] Fortenberry, R. C.; Francisco, J. S. Factors Affecting the Spectroscopic Observation of Bridged HPSi and Linear HSiP in Astrophysical/Interstellar Media. *Astrophys. J.* **2017**, *843*, 124.
[77] Gottlieb, C. A.; Vrtilek, J. M.; Thaddeus, P. Laboratory Measurement of the Rotational Spectrum of SiCC. *Astrophys. J.* **1989**, *349*, L29–L32.
[78] Butenhoff, T. J.; Rohlfing, E. A. Laser-Induced Fluorescence Spectroscopy of Jet-Cooled SiC_2. *J. Chem. Phys.* **1991**, *95*, 1–8.
[79] Dowling, J. M. The Rotation-Inversion Spectrum of Ammonia. *J. Molec. Spectrosc.* **1968**, *27*, 527–538.
[80] Shimanouchi, T. *Tables of Molecular Vibrational Frequencies*, 39th ed.; National Standards Reference Data System: Washington, DC, 1972; Vol. 1.
[81] Jacox, M. E. Vibrational and Electronic Energy Levels of Polyatomic Transient Molecules. *J. Phys. Chem. Ref. Data* **1994**, *23*, 1–461.
[82] Brünken, S.; Gottlieb, C. A.; McCarthy, M. C.; Thaddeus, P. Laboratory Detection of HOCN and Tentative Identification in Sgr B2. *Astrophys. J.* **2009**, *697*, 880.
[83] Fortenberry, R. C.; Huang, X.; Francisco, J. S.; Crawford, T. D.; Lee, T. J. Vibrational Frequencies and Spectroscopic Constants from Quartic Force Fields for *cis*-HOCO: The Radical and the Anion. *J. Chem. Phys.* **2011**, *135*, 214303.
[84] Oyama, T.; Funato, W.; Sumiyoshi, Y.; Endo, Y. Observation of the pure rotational spectra of *trans*- and *cis*-HOCO. *J. Chem. Phys.* **2011**, *134*, 174303.
[85] Bogey, M.; Demuynck, C.; Destombes, J. L.; Krupnov, A. Molecular Structure of $HOCO^+$. *J. Molec. Spectrosc.* **1988**, *190*, 465–474.
[86] Amano, T. Spectroscopic Detection of Protonated N_2O. *Chem. Phys. Lett.* **1986**, *127*, 101–104.
[87] Bogey, M.; Demuynck, C.; Destombes, J. L. Millimeter and Submillimeter Wave Spectroscopy of Protonated and Deuterated Nitrous Oxide. *J. Chem. Phys.* **1988**, *88*, 2108–2111.
[88] Thaddeus, P.; Vrtilek, J. M.; Gottlieb, C. A. Laboratory and Astronomical Detection of Cyclopropanylidene, C_3H_2. *Astrophys. J.* **1985**, *296*, L63–L66.
[89] Dateo, C. E.; Lee, T. J.; Schwenke, D. W. An Accurate Quartic Force-Field and Vibrational Frequencies for HNO and DNO. *J. Chem. Phys.* **1994**, *101*, 5853–5859.

[90] Agbaglo, D.; Fortenberry, R. C. The Performance of CCSD(T)-F12/aug-cc-pVTZ for the Computation of Anharmonic Fundamental Vibrational Frequencies. *Int. J. Quantum Chem.* **2019**, *119*, e25899.

[91] Agbaglo, D.; Fortenberry, R. C. The Performance of Explicitly Correlated Wavefunctions [CCSD(T)-F12b] in the Computation of Anharmonic Vibrational Frequencies. *Chem. Phys. Lett.* **2019**, *734*, 136720.

[92] Huang, X.; Valeev, E. F.; Lee, T. J. Comparison of One-Particle Basis Set Extrapolation to Explicitly Correlated Methods for the Calculation of Accurate Quartic Force Fields, Vibrational Frequencies, and Spectroscopic Constants: Application to H_2O, N_2H^+, $NO_2{}^+$, and C_2H_2. *J. Chem. Phys.* **2010**, *133*, 244108.

CHAPTER IV: NOBLE GASES IN RELATIVELY COMPLEX MOLECULES

A. Introduction

Noble gases have not been found to participate often in molecular bonding, but there are some significant bonds that include noble gas atoms. One particularly interesting molecule is HeH^+ because it is composed of the most abundant elements in the universe even though Helium is not commonly involved in molecular interactions on Earth. Thorfin R. Hogness and E. G. Lunn first synthesized the helium hydride (HeH^+) molecule in 1925 [28], from which chemists in the 1970s speculated that it could be observed in interstellar bodies, and eventually deduced that it was the first molecule formed in the universe [29]. Recently, a spectral line matching that expected for HeH^+ was observed in planetary nebula NGC 7027 using NASA's SOFIA telescope [29] [30]. This accomplishment shows many areas of astrochemistry being used in conjunction as discussed in Chapter I, combining laboratory experiments, computational predictions, and directing the vibrational spectroscope SOFIA based on ground-based rotational spectroscopy [28] [29] [30]. The unique spectra observed in the HeH^+ molecule and the proton-bound $HeHHe^+$ [31] implies that larger combinations of these bonds could create additional distinctive spectra in interstellar bodies like NGC 7027 [30]. However, synthesizing noble gas molecules on Earth is incredibly difficult, evidenced by the lack of experimental data. Computational chemistry ideally can fill in some of the gaps on the path toward astronomically observing such rare molecules.

Helium, Neon, and Argon are chosen to study in this project because they are small enough and have few enough electrons to compute using the methods described previously. Additionally, they are also known to be among the ten most abundant atoms in the universe [32].

Based on the bonding of HeH^+ [30] and brightness of $HeHHe^+$ [31], similar patterns of bonding are designed with common characteristics: two hydrogen atoms and two noble gas (Ng) atoms. For example, $HeHHHe^+$ represents a dimer of the HeH^+ molecule, which has already been observed and determined to be of importance to astrochemistry [29] [30]. Additionally, it contains the most common molecule in the universe in H_2, and the second-most abundant atoms in the universe in He [32], making any potential molecule based on these moieties highly likely to exist in the universe even if relatively rare compared to their constituents. Two main structural isomers are investigated for geometrical optimization: a linear and cyclic combination. These two combinations offer multiple molecules of study by combining the three noble gases included in this project: He, Ne, Ar. This yielded twelve possible molecules shown in Table 3 below:

Table IV.1: Noble Gas Molecules of Interest

Structure	**Molecular Example**	**Possible Formulas**
Cyclic $Ng_2H_2^+$	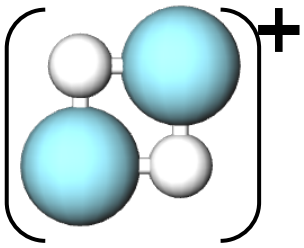	$He_2H_2^+$
		$Ne_2H_2^+$
		$Ar_2H_2^+$
		$NeHeH_2^+$
		$ArHeH_2^+$
		$ArNeH_2^+$
Linear $NgHHNg^+$	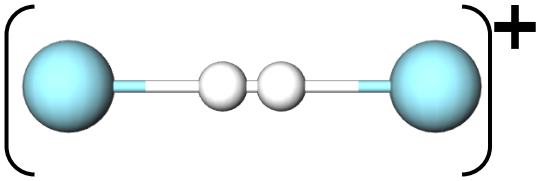	$HeHHHe^+$
		$NeHHNe^+$
		$ArHHAr^+$
		$NeHHHe^+$
		$ArHHHe^+$
		$ArHHNe^+$

Ball-and-stick models are used to represent the large noble gas atoms and small hydrogen atoms. All six combinations were studied in both the cyclic and linear structures.

B. Methods

After narrowing the list of twelve molecules to six linear molecules, the six linear structures were analyzed using the complete CcCR method, followed by the F12-TZ method.

This decision is made in the hopes of showing consistency between the CBS CcCR extrapolation and the explicit correlation of F12-TZ.

The intensities for each molecule's infrared active modes are computed using the MP2/6-31+G level of theory, which optimizes the geometry and computes the intensities of harmonic vibrational frequencies [33]. This level of theory was chosen based on the high speed of computation because the intensity does not rely heavily on the accuracy of the geometry and harmonic frequencies.

C. Results and Conclusions

Table IV.2: F12-TZ and CcCR Vibrational Frequencies (cm^{-1}) and Intensities ($km\ mol^{-1}$)

Molecule	Mode	Symmetry	Description	F12-TZ Harmonic cm^{-1}	CcCR Harmonic cm^{-1}	CcCR Anharmonic cm^{-1}	IR Intensity Km/mol
$HeHHHe^+$	ω_1	σ_g	H-H stretch	2314	2314	2074	
	ω_2	σ_g	symmetric He-H-H bend	397	399	269	303
	ω_3	σ_u	symmetric He-H stretch	279	280		
	ω_4	π_u	antisymmetric He-H stretch	706	706		918
	ω_5	π_g	antisymmetric He-H-H bend	231	228		
$NeHHNe^+$	ω_1	σ_g	H-H stretch	2355	2356	2109	
	ω_2	σ_u	symmetric Ne-H stretch	504	499	—	
	ω_3	σ_g	symmetric Ne-H-H bend	220	219		235
	ω_4	π_u	antisymmetric Ne-H stretch	709	679		2111
	ω_5	π_g	antisymmetric Ne-H-H bend	193	186		
$ArHHAr^+$	ω_1	σ_g	H-H stretch	2280	2274	2429	
	ω_2	σ_u	symmetric Ar-H stretch	924	925	807	
	ω_3	σ_g	symmetric Ar-H-H bend	215	214		62
	ω_4	π_u	antisymmetric Ar-H stretch	800	801		2983
	ω_5	π_g	antisymmetric Ar-H-H bend	192	179		
$NeHHHe^+$	ω_1	σ	H-H stretch	2162	2170	1742	817
	ω_2	σ	Ne-H stretch	760	743	606	1165
	ω_3	σ	He-H stretch	148	149		16
	ω_4	π	Ne-H-H bend	677	650		12
	ω_5	π	He-H-H bend	145	144		229
$ArHHHe^+$	ω_1	σ	Ar-H stretch	1549	1550	1441	1964
	ω_2	σ	H-H stretch	1137	1136	872	394
	ω_3	σ	He-H stretch	79	78		8
	ω_4	π	Ar-H-H bend	662	648		14
	ω_5	π	He-H-H bend	34	26		89
$ArHHNe^+$	ω_1	σ	Ar-H stretch	1621	1613	1308	1805
	ω_2	σ	H-H stretch	1157	1155	1054	379
	ω_3	σ	Ne-H stretch	64	62		20
	ω_4	π	Ar-H-H bend	673	650		10
	ω_5	π	Ne-H-H bend	64	43		99

The results from these six linear molecules' F12-TZ and CcCR QFFs are compiled in Table 4 above. Immediately of note is that only the first two anharmonic CcCR vibrational frequencies for each molecule were reliable enough to include. The other nonincluded frequencies were inconsistent and showed signs of being highly influenced by noise than by clear

computation, but the reported modes were consistent across both QFFs and justified in including in the table.

Given that F12-TZ and CcCR are known to produce vibrational frequencies within 7 cm^{-1} of experimental data, while CcCR produces better rotational constants to within 34 MHz of experimental data [18] [19] [20] [21] [27], Table 4 shows that the F12-TZ Harmonic and CcCR Harmonic frequencies are highly similar, often within a few wavenumbers of each other. This agreement suggests that the harmonic force constants in each method are similar, and the methods likely diverge in the anharmonic treatment in SPECTRO. However, only the first two vibrational modes from these molecules were reported. The other three seemed to reflect large amounts of noise rather than real data because of significant differences between the F12-TZ and CcCR results in addition to non-physical results and questionable behavior. This is likely due to the weak bonding present in many of these systems between the noble gas atom, especially Neon, and the small Hydrogen atom. This is also a consequence of the QFF only reaching the fourth-order expansion; with higher order, the accuracy should increase [5] [6].

A positive anharmonicity is observed in ν_1 for $ArHHAr^+$. This is of concern given the expectation that anharmonic frequencies should be smaller than harmonic frequencies [2], but this result could likely be another effect of the previously described weak bonding in the molecule. Further study should be used to study these lower frequency modes, especially within the vibrational bends of these molecules.

These results are likely useful because they follow the predicted effect of noble gases on known frequencies. Particularly, the anharmonic H-H stretch in the H_2^+ molecule has been found at 2191 cm^{-1} [34], and the addition of noble gas ligands to this structure causes the frequency to drop substantially, as noted across all six molecules' CcCR anharmonic frequencies. This agrees

with quantum chemical theory according to the inverse relationship between mass and frequency. However, the magnitude of this change is harder to predict and did not show a correlation between ligand mass and change in frequency, likely due to other characteristics like bond strength and length. Therefore, these computed frequencies are likely reliable enough to begin comparing with astronomical observations.

Several unique intensities are noticed for these molecules as well. In the three molecules of $HeHHHe^+$, $NeHHNe^+$, and $ArHHAr^+$, only two frequencies are infrared active due to the internal symmetry exhibited. The same vibrational frequency is the most intense in all six molecules, however, the stretch between a noble gas and hydrogen, and this intensity only increases as the mass of the noble gas increases. This suggests that spectroscopic observations of these molecules will show incredibly bright modes at these corresponding frequencies, which can be incredibly useful for molecular identification. The largest intensity across all molecules is found to be 2983 (km/mol) for the antisymmetric Ar-H stretch in $ArHHAr^+$, which is over one order of magnitude larger than the most intense 54-72 km/mol bending mode of water [35]. This $ArHHAr^+$ brightness is uncommonly strong and implies that this stretch in particular will be evident if directly observed using infrared spectroscopy. Some molecules may produce vibrational frequencies in the similar range of the vibrations discussed above so their unique infrared brightness can directly narrow the possible molecules to the ones that occupy both that frequency and intensity.

Table IV.3: CcCR Rotational Constants

Molecule	B_e MHz	B_0 MHz	B_1 MHz	B_2 MHz	D_e	H_e
$HeHHHe^+$	19749	18097	17277	17511	214 kHz	-2274 mHz
$NeHHNe^+$	3358	3282	3150	3057	3522 Hz	-2733 μHz
$ArHHAr^+$	1525	1530	1479	1481	344 Hz	14 μHz
$NeHHHe^+$	9451	8696	7272	9331	141 kHz	-12 Hz
$ArHHHe^+$	5870	5913	5437	5432	135 kHz	-16 Hz
$ArHHNe^+$	1840	1824	1571	1780	7058 Hz	-108 mHz

Given the fact that CcCR QFFs produce more accurate rotational constants than F12-TZ QFFs, only the CcCR rotational constants are included in the table above. The data in this table are likely reliable given that all six molecules share the basic linear geometry and differ in the ligand masses; therefore, theory suggests that the rotational constants should decrease with increased mass, which is consistent from the least massive $HeHHHe^+$ to the most massive $ArHHAr^+$ of the six molecules. Performing another type of QFF, possibly B3LYP, could help support this data being used for identification of these molecules in space.

By using further corrections for higher-order electron correlation and quantum electrodynamics in CcCR QFFs, perhaps the results could become clearer, but such results are unlikely because these changes are most frequently noted in molecules containing atoms beyond the third row while increasing the computational cost and time immensely. Therefore, adding these corrections was deemed unnecessary and inefficient for the project at hand. Computing a global potential energy surface rather than a QFF in this project is one step that should hopefully improve these results.

Upon optimization of the CcCR geometry, the first step in effective QFFs, only the linear structures would actually engage in complete bonding. All six cyclic structures failed to optimize because one noble gas atom bonded to both hydrogen atoms while the other noble gas atom effectively trailed off without bonding. As shown in Figure 1 below, this effectively turns the cyclic structure into another linear structure, $HNgH^+$.

Figure IV.1: Dissociation while Optimizing Cyclic $Ng_2H_2^+$ Molecules

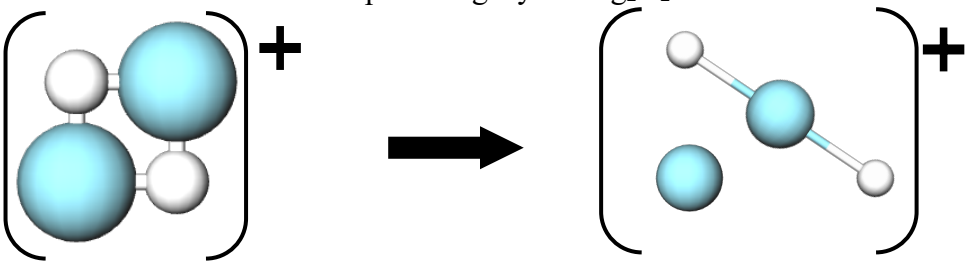

The inability of the proposed cyclic isomers to form an optimized geometry suggests that this cyclic structure is more of an intermediate or transition state of the collision between two NgH^+ molecules than a bonded molecule. While this does not provide useful results for this project, further studies could investigate this collision and other dissociations of these molecules. For example, the differences between $HeHHHe^+$ and $HeHH^+$ may help determine which parts of these molecules are muddying the anharmonic frequencies. The dissociation energies of components like $HeHH^+$, HeH^+, and He could also show the strength of the molecule's full bond. By determining how the frequencies change upon these dissociations, the interaction of these molecules and components may be better observed in highly energetic media, such as nebulae, which would lend insight into possible observation of the complete $NgHHNg^+$ molecules.

CHAPTER V: CONCLUSION

The F12-TZ and CcCR methods have been shown to have applicability in astrochemistry through accurate computation of observable characteristics of astromolecules. F12-TZ is reliable enough for computing vibrational frequencies while CcCR is even more reliable for computing rotational constants of various astromolecules [21] [27]. The accuracy between experimental and computational determination of these characteristics show that computational methods are reliable and effective for the time and cost associated with them. This fine balance has been successful for predicting vibrational and rotational spectra of silicon oxides and various interstellar molecules. This accuracy can also be extended to rare noble gas molecules discussed previously, which suggests that computational methods can be applied to an endless array of molecules that may not have even been imagined yet. Computational astrochemistry has implications not only on finding molecules in tremendous interstellar bodies but also on expanding the breadth of future molecules that can be imagined and eventually synthesized in laboratories.

LIST OF REFERENCES:

1. Barone, V.; Biczysko, M.; Puzzarini, C. Quantum Chemistry Meets Spectroscopy for Astrochemistry: Increasing Complexity toward Prebiotic Molecules. *Accounts of Chemical Research* 2015, *48* (5), 1413–1422.
2. Sathyanarayana, D. N. *Vibrational spectroscopy: theory and applications*; New Age International: New Delhi, 2004.
3. Galabov, B.; Dudev, T.; Durig, J. R.; Orville-Thomas, W. J. Computations in Vibrational Intensity Spectroscopy. *Journal of Molecular Structure* 1988, *173*, 111–128.
4. NASA Under the Spotlight: The Decade-Late, Over-Budget Arrival of SOFIA Shows That NASA's Practices Need to Change. *Nature* 2010, *466* (7305), 413–413.
5. C.J. Cramer, Essentials of Computational Chemistry: Theories and Models, second ed., Wiley, West Sussex, England, 2004.
6. T.J. Lee, J.M.L. Martin, P.R. Taylor, An accurate ab initio quartic force field and vibrational frequencies for CH_4 and its isotopomers, J. Chem. Phys. 102 (1995) 254-261.
7. Fortenberry, R.C., Lee, T.J., 2019. Computational vibrational spectroscopy for the detection of molecules in Space. Annu. Rep. Comput. Chem. 15, 173–202.
8. Raghavachari, K., Trucks, G.W., Pople, J.A., Head-Gordon, M., 1989. A fifth-order perturbation comparison of electron correlation theories. Chem. Phys. Lett. 157, 479–483.
9. Shavitt, I., Bartlett, R.J., 2009. Many-body Methods in Chemistry and Physics: MBPT and Coupled-Cluster Theory. Cambridge University Press, Cambridge.
10. Hill, J.G., Peterson, K.A., 2010. Correlation consistent basis sets for explicitly correlated wavefunctions: valence and core-valence basis sets for Li, Be, Na, and Mg. Phys. Chem. Chem. Phys. 12, 10460–10468.

11. Prascher, B.P., Woon, D.E., Peterson, K.A., Dunning, T.H., Wilson, A.K., 2011. Gaussian basis sets for use in correlated molecular calculations. VII. Valence, core-valence, and scalar relativistic basis sets for Li, Be, Na, and Mg. Theor. Chem. Acc. 128, 69–82.
12. Werner, H.-J., Knowles, P.J., Knizia, G., Manby, F.R., Schütz, M., 2012. Molpro: a general-purpose quantum Chemistry program package. WIREs Comput. Mol. Sci. 2, 242–253.
13. Werner, H.-J., et al., 2015. MOLPRO, version 2015.1, a package of ab Initio Programs. see. http://www.molpro.net.
14. J.M.L. Martin, P.R. Taylor, Basis set convergence for geometry and harmonic frequencies. Are h functions enough?, Chem. Phys. Lett. 225 (1994) 473–479.
15. M. Douglas, N. Kroll, Quantum electrodynamical corrections to the fine structure of helium, Ann. Phys. 82 (1974) 89–155.
16. G. Jansen, B.A. Hess, Revision of the Douglas-Kroll Hamiltonian, Phys. Rev. A 39 (1989) 6016–6017.
17. R.C. Fortenberry, X. Huang, J.S. Francisco, T.D. Crawford, T.J. Lee, The trans- HOCO radical: fundamental vibrational frequencies, quartic force fields, and spectroscopic constants, *J. Chem. Phys*. 135 (2011) 134301.
18. D. Agbaglo, R.C. Fortenberry, The performance of CCSD(T)-F12/aug-cc-pVTZ for the computation of anharmonic fundamental vibrational frequencies, Int. J. Quant. Chem. 119 (2019) e25899.
19. D. Agbaglo, R.C. Fortenberry, The performance of explicitly correlated wavefunctions [CCSD(T)-F12b] in the computation of anharmonic vibrational frequencies, Chem. Phys. Lett. 734 (2019) 136720.

20. X. Huang, E.F. Valeev, T.J. Lee, Comparison of one-particle basis set extrapolation to explicitly correlated methods for the calculation of accurate quartic force fields, vibrational frequencies, and spectroscopic constants: application to H2O, N2H+, NO+2, and C2H2, J. Chem. Phys. 133 (2010) 244108.
21. Gardner, M. B.; Westbrook, B. R.; Fortenberry, R. C.; Lee, T. J. Highly-Accurate Quartic Force Fields for the Prediction of Anharmonic Rotational Constants and Fundamental Vibrational Frequencies. *Spectrochimica Acta Part A: Molecular and Biomolecular Spectroscopy* 2021, *248*, 119184.
22. X. Huang, T.J. Lee, A procedure for computing accurate Ab initio quartic force fields: application to HO2+ and H2O, J. Chem. Phys. 129 (2008) 044312.
23. W.D. Allen, coworkers, INTDER 2005 is a General Program Written by W.D. Allen and Coworkers, which Performs Vibrational Analysis and Higher-Order Non-Linear Transformations, 2005..
24. J.F. Gaw, A. Willets, W.H. Green, N.C. Handy, in: J.M. Bowman, M.A. Ratner (Eds.), Advances in Molecular Vibrations and Collision Dynamics, JAI Press Inc, Greenwich, Connecticut, 1991, pp 170–185..
25. D. Papousek, M.R. Aliev, Molecular Vibration-Rotation Spectra, Elsevier, Amsterdam, 1982.
26. J.M.L. Martin, P.R. Taylor, Accurate ab initio quartic force field for trans-HNNH and treatment of resonance polyads, Spectrochim. Acta A 53 (1997) 1039– 1050.
27. Gardner, M. B.; Westbrook, B. R.; Fortenberry, R. C. Spectral Characterization for Small Clusters of Silicon and Oxygen: SiO2, SiO3, Si2O3, &; Si2O4. *Planetary and Space Science* 2020, *193*, 105076.

28. Helium hydride. https://www.acs.org/content/acs/en/molecule-of-the-week/archive/h/helium-hydride.html (accessed Mar 24, 2021).

29. Lemonick, S. Universe's First Molecules Finally Found in Space. *C&EN Global Enterprise* 2019, *97* (16), 5–5.

30. Güsten, R.; Wiesemeyer, H.; Neufeld, D.; Menten, K. M.; Graf, U. U.; Jacobs, K.; Klein, B.; Ricken, O.; Risacher, C.; Stutzki, J. Astrophysical Detection of the Helium Hydride Ion HeH+. *Nature* 2019, *568* (7752), 357–359.

31. Fortenberry, R. C.; Wiesenfeld, L. A Molecular Candle Where Few Molecules Shine: HeHHe+. *Molecules* 2020, *25* (9), 2183.

32. McCall, B.J., 2006. Dissociative recombination of cold H_3^+ and its interstellar implications. Phil. Trans. Royal Soc. A 364, 2953–2963.

33. Balci, K.; Akyuz, S. A Vibrational Spectroscopic Investigation on Benzocaine Molecule. *Vibrational Spectroscopy* 2008, *48* (2), 215–228.

34. CCCBDB Listing of experimental vibrational data for H_2^+ (Hydrogen cation). https://cccbdb.nist.gov/expvibs2x.asp#webbook (accessed Mar 24, 2021).

35. Bégué, D.; Baraille, I.; Garrain, P. A.; Dargelos, A.; Tassaing, T. Calculation of IR Frequencies and Intensities in Electrical and Mechanical Anharmonicity Approximations: Application to Small Water Clusters. *The Journal of Chemical Physics* 2010, *133* (3), 034102.